GFAP Proteolysis in TBI: Linking Novel Modified Cleavage Products to Astrocyte Pathology and Patient Outcomes

Ina-Beate Wanner[1*], Julia Halford[1], Jonathan Lopez[1], Sean Shen[2], Yu Chen[3], Hayden Zhao[1], Carolina I. Salas[1], Rachel R. Ogorzalek Loo[2], Steven Robicsek[4], Benjamin M. Ellingson[5], Jeffrey Gornbein[6], Timothy E. Van Meter[7], Gerry Shaw[8,9], Joseph A. Loo[2], and Paul M. Vespa[10].

*Corresponding Author.
1: Semel Institute for Neuroscience and Human Behavior, Intellectual and Developmental Disability Center (IDDRC) and Brain Injury Research Center (BIRC); 635 Charles E. Young Drive South, NRB315, David Geffen School of Medicine, UCLA, Los Angeles, CA 90095-7332, CA, USA; IWanner@mednet.ucla.edu.
2: Dept. of Chemistry and Biochemistry, Molecular Biology Institute, David Geffen School of Medicine, UCLA.
3: Molecular Instrumentation Center (MIC), Dept. of Chemistry and Biochemistry, UCLA.
4: Dept. of Anesthesiology, University of Florida, Gainesville, FL 32610-0254.
5: Dept. of Radiologial Sciences, Geffen School of Medicine, UCLA.
6: Dept. of Computational Medicine, Statistics Core of the Dept of Medicine, School of Public Health, UCLA.
7: BRAINBox Solutions, Inc., Richmond, VA 23219.
8: Dept. of Neuroscience, University of Florida College of Medicine, Gainesville, FL 32610.
9: EnCor Biotechnology Inc., Gainesville, FL, 32608.
10: Dept. Neurology and Neurosurgery, BIRC; David Geffen School of Medicine, Ronald Reagan Medical Center, UCLA.

Abstract

Monitoring patients with traumatic brain injury (TBI) is essential for mitigating secondary complications. TBI disrupts proteostasis, leading to increased protein degradation and proteinopathy, which heighten the risk of neurodegeneration and underscore the need for early detection via noninvasive biomarkers. Glial fibrillary acidic protein (GFAP), an astroglial intermediate filament, is a well-established TBI biomarker, yet pathomechanisms and proteoforms of GFAP release are incompletely understood. This translational study defined the GFAP degradome in TBI through mass spectrometry (MS) sequencing of immunopurified GFAP breakdown products (BDPs) from patient biofluids. The TBI-GFAP fragments differed from those of Alzheimers and Alexander Diseases, revealing novel coil1/coil2-harboring cleavage products in TBI CSF, while TBI serum samples had only coil1-products. Trauma-specific citrullinations and acetylations were validated via MS spectra. Epitope mapping identified a novel trauma-specific cleavage site and revealed coil1-BDPs as selectively released into fluid, while coil2 fragments remained intracellular in a human trauma culture model. Citrullinated GFAP-specific antibodies exhibited distinct binding patterns from those of unmodified, native GFAP in TBI patients CSF and detected unique granular aggregates in dystrophic astrocytes without staining filamentous GFAP. TBI-GFAP fragments were produced by stepwise trauma-activated calpain and caspase activities shown by in vitro inhibitor studies. Live cell

imaging with fluorescent protease reporters demonstrates coexisting calpain and caspase activities, along with membrane disruption jointly identifying distinct astrocyte injury states. The trajectory of GFAP proteolysis was analyzed in CSF samples from 24 TBI patients over 10PIDs, via calibrated, band-specific scaled immunoblot densitometry. These profiles covaried with patient age and body temperature. Full-length GFAP and 45-49kDa fragments peaked on injury day and declined over time, whereas calpain-generated 37-39kDa BDPs remained elevated. Small BDPs exhibited either delayed rises or remained undetected. Compared to the 20-26kDa BDPs, 15-19kDa products were notably underrepresented, consistent with coil1-BDPs preferred release and coil2-BDPs selective cellular retainment. Fluid levels of calpain-generated GFAP fragment were time and severity-dependent in the trauma culture model. TBI CSF trajectories of GFAP-BDPs differentiated TBI patients with poor versus those with good outcomes on the extended Glasgow Outcome scale (GOSE), whereas uncleaved GFAP trajectories failed in early prediction of patient outcome at six months. These findings define trauma-specific GFAP degradome dynamics and highlight novel longitudinal proteolysis profiles for patient monitoring and stratification. This work is significant as it supports GFAP fragment profiling for potential context of use (COU) in neurocritical care TBI monitoring, and offers preliminary insights into diagnosing astroglial proteinopathy-linked neurodegeneration after TBI.

Introduction

Traumatic brain injury (TBI) is the most common neurological disorder surpassing Alzheimer's disease and stroke with a global prevalence of 56 million cases annually[1]. A rigorous meta-analysis showed that 18 % of the adult US population suffered a TBI with loss of consciousness during their lifetime[2]. Among survivors, 53% of mild TBI and 85% of moderate-to-severe TBI patients fail to achieve long-term recovery[3,4]. TBI recovery is profoundly shaped by secondary injury mechanisms, as an initial trauma disrupts cerebral homeostasis, which amplifies neural and biochemical dysfunction[5,6]. Effective monitoring of patients with TBI is therefore critical to minimize exacerbation and attenuate secondary injury processes. Although intracerebral catheters provide valuable information, their placement is invasive and reporting remains focal and is reserved for patients undergoing surgical intervention[7,8]. Thus, developing biomarkers for wide use to noninvasively monitor, evaluate, and improve outcome prediction in a broad spectrum of TBI patients is of high interest[9].

The FDA has approved a blood test that includes glial fibrillary acidic protein (GFAP) for use within 12 hours (hrs) post-injury to detect brain abnormalities typically identified by CT scan among patients with mild TBI Glasgow Coma Scale score of 13-15[10,11]. This narrow context of use (COU) excludes a wider population of TBI patients and does not address longitudinal patient monitoring[12,13]. To improve TBI patient evaluation, the National Institute of Neurological Disorders and Stroke (NINDS) has recently introduced a new TBI Classification framework that integrates biomarkers such as GFAP, and other assessment tools[14,15]. Effective broader use of GFAP to inform and guide future clinical applications for patient monitoring and stratification requires an understanding of GFAP's fate during TBI pathophysiology[16]. Two key interrelated questions remain: (1) What are the pathobiological underpinnings of GFAP signals in TBI? (2) What is the temporal dynamic of GFAP release and degradation following TBI?

The astroglial intermediate filament protein GFAP is highly enriched in the brain and is well studied, both as a biofluid marker and as a neuropathology indicator of reactive astrogliosis. GFAP levels are elevated in CSF and blood in patients with intracranial injuries such as hemorrhage, as observed in brain CT scans[10,17,18]. Elevated serum GFAP levels have been shown to predict poor outcome and mortality after TBI[9,19-21]. Therefore, GFAP is extensively investigated as a diagnostic and prognostic biomarker for TBI evaluation in clinical trials and translational studies. GFAP levels in biofluids are transient, rise within hrs after injury, reach their peak 6-18hrs post-injury, and then decline[21-24].

It is not well understood how a filament-tethered protein appears rapidly in circulation and how proteases shape GFAP fluid profiles. This requires integrating longitudinal biochemical analysis of GFAP degradation and post translational modifications (PTMs) with insights into cellular injury states[16].

In this translational research study we determined novel proteolytic breakdown products (BDPs) of GFAP and trauma-induced PTMs in TBI patients. Using a unique human cerebral trauma culture model we link these trauma-proteoforms to astrocyte injury states and trauma-activated proteases. Mass spectrometry (MS) of immunopurified GFAP fragments from TBI patient CSF identified, for the first time, a set of TBI-generated GFAP BDPs with citrullination and acetylation modifications. Some groups of GFAP BDPs were preferentially released while others were selectively retained. We tracked longitudinal GFAP degradation patterns in Neuro-ICU patients and demonstrate fragment-specific correlations with six-month outcomes. This work conceptually connects GFAP biofluid patterns to an underlying non-filamentous proteinopathy, to astrocyte injury states, and neurodegeneration. These new insights into GFAP degradation, modification, and fate of specific GFAP proteofoms support a future for their broader clinical use.

Methods

TBI patients, demographic and clinical data and brain tissue specimen: The study comprised 112 CSF samples and 3 serum samples from 26 TBI patient and one control (Precision Med), average age 42±19, 22 male and 4 female. Their Glasgow Coma Scale (GCS) averaged a score of 6.6 ±3.4 along with anonymous demographic and clinical parameters (Suppl.Tables1,2). Human subjects protocols for the DANA foundation funded cohort included local IRB approved informed consent procedures from three medical centers (1) UCLA Ronald Reagan Hospital Neuro-Intensive Care Unit (Principal Investigator, PI Dr. Paul Vespa) and (2) University of Florida Dept of Anesthesiology (PI Dr. Steven Robicsek). Deidentified human fetal brain tissue from voluntarily aborted pregnancies was donated adhering to stringent ethical regulations. They were pre-shelved (exempt from IRB-review) at the UCLA Translational Pathology Core Laboratory (TPCL; tissue procurement by Dr. Sara Dry). Consent was established through UCLA Family Planning Services, Dept of OB-GYN (Dr. Angela Chen). Signed informed consent occurred after decision on elective termination, complying with US Public Law 103-43 and NIH policy, ensuring no incentivizing (The Public Health Service Act, 42 U.S.C. § 289g-2). Cerebral astrocyte cultures were prepared from 17 donated human fetal cranial specimen aged 16-19.5 gestational weeks.

Immunoprecipitation and mass spectrometry (MS) sequencing of GFAP from TBI patients:

MS experiments were performed on six CSF and serum samples from five TBI patients. GFAP was immunoprecipitated using a rabbit polyclonal anti-GFAP antibody that was cross-linked to protein G conjugated magnetic beads (Dynabeads) using dimethylpimelimidate-2 (freshly prepared 20mM DMP in 200mN triethanolamine, ph8.6) followed by heat/ice denaturing and reduction in 1% ß-mercaptoethanol to maximize yield[25-27]. Eluted material was separated by preparative SDS-PAGE using 10% NuPAGE gradient gels in morpholinoethansulfonic acid (MES) buffer in reducing conditions along with a molecular weight standard (Benchmark). Gels were Sypro-Ruby stained and fixed in 10% methanol, 7% acetic acid. GFAP bands were cut out under UV light and placed into tubes for in-gel trypsin digestion. A fraction (~1/9th) of the eluate was blotted and GFAP was detected using a mouse monoclonal GFAP antibody (mab1A64-244, Abbott Diagnostics or MCA3E10, EnCor Biotechnology Inc.) to provide reference signals for gel band excision. Bands at 50 and 25kDa were omitted to avoid immunoglobulins (Supplemental Figure 1). Gel bands were fully destained, dried, and then reduced with 10 mM tris(2-carboxyethyl) phosphine in 100 mM ammonium bicarbonate buffer at 56°C for 30min followed by alkylation with 100 mM iodoacetamide in the same buffer at 37°C for 15min. The bands were equilibrated with acetonitrile (ACN), dried, and and digested using 0.01mg/ml sequencing grade trypsin in 100mM ammonium bicarbonate buffer at 37°C for 12hrs. Peptides were extracted from the gel bands by three rinses of 50% ACN/0.1% formic acid solution at 37°C for 15 min and the combined extracts were dried in a vacuum concentrator. The peptides were measured by liquid chromatography-tandem MS (LC-MS/MS) using an Ultimate 3000 nano LC instrument (1-hr gradient) coupled to a Q-Exactive Plus Orbitrap mass spectrometer. Full spectra (MS1) were collected at a resolution of 70,000 and the 15 most abundant ions of each scan were subsequently fragmented by higher-energy collisional dissociation (HCD; MS2) with a resolution of 17,500 and a dynamic exclusion of 45 seconds. Varied amounts of recombinant human GFAP were employed as technical controls. Raw MS data were searched against the human GFAP protein sequence (Uniprot (https://www.uniprot.org/uniprotkb/P14136/entry) by Proteome Discoverer (PD) version 1.4. SEQUEST-engine searches of the peptides confirmed that the sequences are unique to GFAP, excluding other proteins (e.g., vimentin, neurofilaments). GFAP sequence map regions marked green show "high" confidence filtering with at least two peptides per region and ≤1% false discovery rate (FDS) correction for Xcorr Score versus charge; while only few regions marked yellow were detected by at least two "medium" confident peptides with ≤5% FDR (Figure 1). Identified PTMs including acetylation and citrullination were further validated by: (a) unique signatures of citrullination (immonium ion at m/z 130.0975 and/or neutral loss of isocyanic acid at 43.0058 Da) or lysine acetylation (cyclized immonium ion at m/z 126); (b) MS2 product ions (b/y) revealing mass increments consistent with modification (Supplemental Figure 9); (c) comparison of identified citrullination sites after treatment with peptidylarginine deiminase (PAD) enzyme[28].

Partial chemical cleavage of GFAP for monoclonal antibody epitope mapping: The binding region of monoclonal anti-GFAP clone 5C10 was determined initially by binding to the peptide covering amino acids 233-261 of the human coil 2A sequence (AALKEIRTQYEAMASSNMHEAEEWYRSKF) using dot blotting (not shown). The specific epitope was subsequently identified using partial chemical cleavage at the single tryptophan in GFAP, amino acid W256. Recombinant GFAP (33µg, EnCor Biotechnology Inc.) was treated in excess with 1% BNPS-Skatole (100µg; 1mg/ml glacial acetic acid; 3-bromo-3-methyl-2-(o-nitrophenylsulfenyl)indolenine, Sigma), an oxidant and brominating agent that cleaves proteins at tryptophan residues[29,30]. An equal volume of distilled water precipitated BNPS-Skatole and was removed by centrifugation (5min at 12,000rpm). The supernatant was

lyophilized and the GFAP and tryptophan-cleaved BDPs were separated by SDS polyacrylamide gel electrophoresis (SDS-PAGE) blotted followed by antibody incubation of MCA 5C10 and a pan-intermediate filament antibody, IFA (hybridoma supernatant from ATCC, epitope coil2B aa 358-377: ALDIEIATYRKLLEGEENRI) [31,32].

Western blotting using scaled densitometry and biomarker calibration: SDS-PAGE was conducted as previously described using 7.5% acrylamide for αII-spectrin, 12% gels for GFAP[23]. Protease inhibitors (cocktail CompleteMini, Roche 1:50) and EDTA to a final concentration of 10mM were added to TBI patient CSF and the samples were added to Laemmli sample buffer, boiled for 5min followed by ice incubation and addition of ß-mercaptoethanol to 1%, prior to loading 34 µl/lane. The same procedure was followed for astrocyte lysates and concentrated media was prepared as described below. Samples and molecular weight standards (Kaleidoscope, Biorad) were collected upon initial run for 30min at 100V and separated for 1h at 120V until the bromophenol blue front reached the gel bottom. Proteins were cold transferred at 120V for 3hrs onto nitrocellulose and stained with Ponceau S. Membranes were blocked in 10% non-fat milk in Tris-buffered saline with Tween (TBST) at room temperature (RT) prior to incubation with primary antibody in 5% bovine serum albumin (BSA) in TBST overnight at 4°C. Secondary antibodies conjugated with peroxidase (Pierce) were incubated in 5% BSA in TBST for 1hour at RT. Enhanced Chemiluminescence (ECL) substrate was applied to washed membranes for 5min at RT (Pico and Femto ECL)and multiple exposures of Kodak films as well as an iBright imager were used. Calibrants were recombinant human full-length GFAP and a 20kDa His-tagged BDP (72-217, EnCor Biotechnology Inc.) that were diluted with 0.5% BSA as carrier in Tris-buffered saline (TBS) at various concentrations ranging from 0.08ng-2.6ng that were measured at different exposures (Supplemental Figure12). Densitometry was done on eight exposures of each blot (2s-20min) after background correction. Sub-saturated band measurements were standardized to 1min by multiplying shorter exposures and by dividing longer exposures using scaling factors between exposures that were empirically determined from same unsaturated bands found on two exposures (Supplemental Table 5). This stepwise scaling corrected for limitations of enzyme-substrate reaction and film saturation and expanded the detection range continuously over 5 orders of magnitude. Band sizes were computed using distances of each molecular weight marker from the gel-front and curve-fit equations.

Human neocortical astrocyte cultures, trauma, imaging: This human culture trauma model uses in vitro differentiated fetal neocortical astrocytes as previously described[33]. Briefly, neocortical tissue was mechanically dissociated, filtered and astrocytes were enriched by Percoll gradient centrifugation. Cells were expanded in DMEM/F12 with 10% fetal bovine serum (FBS). Residual oligodendrocytes and progenitor cells were removed by shaking. Astrocytes were seeded on collagen I coated deformable silastic membranes at 138,000-180,000 cells/9.62cm^2 and differentiated in DMEM/F12: Brainphysiology Medium supplemented with SM1 and N2A (Stem Cell Technologies) by stepwise serum removal. Astrocytes were traumatized by 50ms pressure pulses (4.9-5.3psi) that abruptly stretched the culture bottom, shearing the cells. This inflicts membrane integrity compromise and delayed cell death[23].

Live microscopy imaging: Cerebral fetal human brain cells were differentiated for three weeks by serum withdrawal in a 1:1 mixture of DMEM/F12: brainphysiology medium (StemCell Technology). Live imaging was done 5hrs after stretch injury on a Leica DMI8 microscope in a gas and temperature-

controlled chamber (Okolab). Cells were bathed for 5min in 60μM propidium iodide (PI, Sigma) to label leaky membranes. Washed cultures were live-imaged in the presence of two permeable fluorescent protease substrate reporters for calpains (30μM CMAC tBoc Leucyl-methionine, ThermoFisher), and for caspases (5μM DEVD-NucView488, Biotium).

Astrocyte protein sample preparation for gel electrophoresis. Whole cell lysate (WCL) of adherent astrocytes was prepared by adding 150μl lysis buffer/9.62 cm^2 wells (150mM NaCl, 20mM Tris, 5mM EDTA, 10mM NaPyrophosphate, 30mM phosphatase substrate, 5mM dithiotreitol, DTT (Calbiochem)), 1% NP40 and 1 tablet/10ml protease inhibitors (Mini Protease Inhibitor Cocktail, Roche). Lysis buffer was incubated for 5min at 4°C, collected by scraping into low binding tubes and homogenized by 3x5sec sonification bursts without foaming (Branson Digital Sonifier, 90% or constant amplitude duty cycle, output level 5). Culture medium without serum or protein supplements was collected and 5mM DTT and 1tablet protease inhibitors /10ml added. Particles from lifted cells and debris were pelleted by initial centrifugation (5000g, 5min, 4°C) then lysed for 5-10 min in 0.5% lysis buffer and sonicated 3x5sec. Remaining insoluble fractions were removed by centrifugation (10min at 16,000g 4°C). Media were concentrated (Vivaspin, 3kDa cutoff) by centrifugation (4-8h at 5000g, 4°C) to ~1/10th-20th of original volume to obtain 1-1.5 μg/ml protein concentration. All samples were immediately frozen at -80°C in aliquots.

Antibodies used on TBI CSF and astrocyte samples: All antibodies used with their known epitopes, sources and dilutions are tabulated with approved RRIDs (Suppl.Table3). A rabbit polyclonal GFAP antibody (DAKO) was used for immunoprecipitation and immunoblotting. For densitometry the antibody was applied in two steps, high dilution (1:20,000-150,000) for detecting full-size GFAP and large GFAP BDPs, followed by a higher concentration (1:5,000-7,000) for detecting small GFAP products followed by scaling for adjustment (see below). A mouse anti-GFAP monoclonal antibody, MCA-3E10 (EnCor Biotechnology Inc.), was generated to a recombinant construct containing amino acids 72-217 of human GFAP, the entire coil1A and 1B sequence. The epitope for MCA-3E10 was localized to amino acids 196-210 (EIRFLRKIHEEEVRE), using peptide competition with a set of nested 20 amino acid peptides, each overlapping by 5 amino acids. Additional antibodies clones were MCA-5C10 (EnCor Biotechnology Inc.), mab1A64-244 (Abbott Diagnostics), a mixture of three clones (4A11, 1B4, 2E1, BD Pharmingen) and mabGA5 (Sigma[34,35]). Citrullination studies used clone CTGF-1221 that was kindly provided by Dr. Akihito Ishigami (Tokyo Metropolitan Institute for Geriatrics and Gerontology) to detect citrullinated GFAP at R270 and R416[36]. Anti-peptidyl-citrulline antibody clone F95 (EMD Millipore) validated citrullinations. Several additional rabbit polyclonal citrullination site-specific GFAP antibodies, including cit-GFAP-270, were generated and characterized (BRAINBox Solutions, Inc.). A mouse antibody to αII-spectrin was used at 1:3,000-1:5,000 dilution (Enzo Life Sciences).

Protease inhibition of traumatized human astrocytes: Pan-calpain inhibitor calpeptin (Z-Leu-nLeu-H, Millipore/Sigma), a cell permeable peptide aldehyde inhibitor[37,38] was specific to calpain 1 without introducing toxicity, and was used at 13μM. Pan caspase inhibitor ZVAD-FMK (Benzyloxycarbonyl-Val-Ala-Asp(OMe)-fluoromethylketone (Enzo/ThermoFisher) is a cell-permeable, irreversible pan-caspase inhibitor effective against a spectrum of caspases (1-10, except 2; Invitrogen)[39]. ZVAD-FMK is reported showing also calpain inhibition after controlled cortical impact to the mouse brain[40]. Here ZVAD-FMK was used at 11μM. Inhibitors were applied 10min to cultures

after stretching in the absence of gentamicin in the medium for 5, 24 or 48hrs and were replenished every 8-10hrs. Other tested calpain inhibitors such as leupeptin (20μM) and SJA6017 (10μM Calpain Inhibitor VI, Calbiochem) had limited effect, or were harmful by either increasing cell permeability as did PD1500606 (100 μM, Calbiochem) or elevating cell death as did MDL28170 (Z-Val-Phe-al, 4μM, Calbiochem; data not shown) and were not further pursued.

Statistics: All GFAP band measurement residuals were assessed for normality by the Shapiro Wilk criterion for Gaussian distribution fit. Due to significant lower W-values, all GFAP measurements were log-transformed replacing zero with half of the lower limit of detection, which was 0.7pg in 22μl CSF or a concentration of 27pg/ml using a polyclonal GFAP antibody. **Reproducibility** of immunoblot densitometry was determined on technical replicates using the coefficients of variation (CV=SD/mean x100). The average between-experiment CV was 27.8% (n=6 pairs of multiple scaled measurements, specifically 37% for full-length GFAP, 21.5% for fragment bands and 25% for 37kDa band). **Covariates**: Patient age, race, sex, and concurrent body temperature and their interactions as well as temperature interaction with postinjury elapsed time were evaluated as potential covariates for GFAP levels by using restricted maximum likelihood (REML) linear mixed model (LMM) with patient identifiers (IDs) as random effect and knotted spline modeling of injury elapsed days (Suppl.Fig.12 for data distribution). Partial omega squared (ω^2) was used to report the proportion of population variance fixed effects as it adjusts for variable sample size (age effect shown for GFAP bandsets in Suppl.Table6)[41]. It was computed using fixed effect F-statistic (F) results of the REML LMM output in SAS/Jmp along with degrees of freedom (df) and its demoninator term (DFDen) for the respective covariate effects following:

$$\omega^2 = \mathrm{F} * \mathrm{df}_{\mathrm{effect}} - (\mathrm{df}_{\mathrm{effect}}/\mathrm{F} * \mathrm{df}_{\mathrm{effect}}) + \mathrm{DFDen} + \mathrm{df}_{\mathrm{effect}}.$$

For Glasgow Outcome Scale Extended (GOSE), demographic covariates were assessed and included in the linear mixed model was patient age as it was covariate for GFAP levels and GOSE outcome. **Temporal profiles:** Longitudinal means were graphed by spline fit lines from resampled daily CSF draws, weighting observations, along with 95% confidence intervals (Figs. 7C,8). Temporal GFAP and fragment trajectories were evaluated using REML-LMM with age and concurrent body temperature as indicated (Suppl.Table6 and Suppl.Fig.13). Cohen's D effect sizes on each postinjury day (PID) were computed using adjusted means (Adj. Mean) on each PID compared with overall means weighted for sample availability on each day[42,43].

$\mathrm{Cohen's\ D}_{\mathrm{forGRAP\ by\ PID}} = (\mathrm{Adj.\ Mean}_{\mathrm{PID}} - \mathrm{Adj.\ Mean}_{\mathrm{Overall}})/\sqrt{pooled\ SD}$, where the pooled standard deviation (SD) was the random variance component (Suppl. Table 8, Suppl.Fig.10)[44].

Multivariate correlation matrix: To assess GFAP substrate-product and product-product relationships, log-transformed GFAP bands were pairwise correlated reporting uncorrected Pearson correlation coefficients (Figure 9, Suppl.Fig.14). Biplots use orthogonal fit for equal variance between GFAP bands were reported with R^2 and false discovery rate (FDR)-corrected Logworth, $-\log_{10}$(p-value) to differentiate highly correlated GFAP bands (Fig. 9). Outlier portion is documented with robust correction defined as percentage of datapoints with a distance exceeding 3X the residual SD. Outliers that might affect the correlations across all variables were reported using the Mahalanobis distance with threshold (upper control limit, UCL) calculated using sample size and the number of variables used, by applying robust weighting to better discern outliers[45-47]. **Outcome prediction:** The GOSE score was used to assess six months recovery prediction by longitudinal GFAP profiles. GFAP

trajectories are shown for good (GOSE 5-8), and poor (GOSE 1-4) outcomes using bootstrapped cubic splines with same curvature fit and 95% confidence bounds λ= 0.28 (Figure 10). GFAP profiles were assessed for distinguishing good versus poor outcome using REML-LMM model with ID as random and elapsed PIDs with knotted splines as fixed effects, adding age as joint covariate. Differences in GFAP Adjusted Means between good and poor recovering patients were computed using $\text{Cohen's D}_{\text{forGFAP by outcome}} = (\text{Adj. Mean}_{\text{GOSE poor}} - \text{Adj. Mean}_{\text{GOSE good}})/\sqrt{pooled\ SD}$ in standard deviational (SD) units using the residual variant component capturing within-subject variability (Suppl.Table7). Inserts in Figure 7 show least square means model adjusted means with standard errors and post-hoc t-statistics and patient ID as random effect and time as fixed effect. **Label-free MS analysis** used A) Peptide presence/absence frequency was compared between coil1 and coil2 peptides using a mixed model with unequal variances, patient ID as random and GFAP-BDP sets as fixed effects. B) The peak ion abundance of coil1 versus coil2 ions was compared using a mixed model analysis with ID as random and fragments as fixed effects while undetected peptides were excluded (Suppl.Fig.2).

Results

Novel set of trauma-specific GFAP breakdown products (BDPs) in TBI patients

GFAP fragments in TBI patients differ from Alzheimers and Alexander Disease BDPs: As GFAP shows many degradation products and TBI facilitates proteolysis, we interrogated TBI-specific GFAP degradation by MS sequencing fragments from gel-slices of immunopurified GFAP of six CSF samples/five TBI patients covering key molecular weight ranges aligned with matching immunoblot GFAP signals (Suppl.Fig.1, Bandsets I-IV). Molecular masses were estimated after pooling slice-specific sequences from all patient samples based on high confidence identified tryptic peptides covering the majority of the fragment sequences in the identified GFAP-BDPs (Fig.1B). Band I contained a 41.7kDa fragment. Band II gel-slice ran between 36-39kDa yet sequenced peptides covered a calculated mass of 40.6kDa. This slightly higher mass than suggested by the gel migration resulted from pooling the peptides of all patient samples. Hence, the larger peptide range suggest patient-specific variability in GFAP proteolysis. Remaining charged residues in the head and tail regions of acidic GFAP may have also contributed to slightly faster gel migration[48-51]. Band III comprises two GFAP-BDPs, a 21.8kDa product from coil1 and a 17.5kDa product from coil2 of the GFAP rod. Band IV also includes coil1 with a slightly shorter, 21.3kDa product and also coil2 with an estimated 15.2kDa product. Coil1-covering fragments display the same N-terminus and slightly differing C-termini producing a four-residue larger Band III and a shorter Band IV coil1 product (Fig. 1C). These coil1 products both extend beyond the previously reported caspase 6 cleavage product associated with Alexander disease at VELD225[34]. Two coil2 product sequences with the same N-terminus (F261) and distinct C-termini, K410 (Band III) and R390 (Band IV) comprise coil2 products differing by 22 amino acids or ~2.4kDa (Fig. 1C). Notably, TBI patient associated15-17.5kDa coil2 products are smaller than the 30kDa fragment associated with Alzheimer's disease, yet consistent with the reported caspase 3 cleavage site (residues 258-266, RSKFA↓DLTD) [52]. Interestingly, no peptides from the linker region between coil1B and 2A and the coil2A region were detected by MS in these small BDPs. Yet these aa were readily detected in larger fragments (not shown) and in control analysis of full-length recombinant GFAP (Suppl.Fig.2). Immunoblots using a polyclonal antibody

detected small GFAP-BDPs with these observed molecular masses, although monoclonal MCA-3E10, specific for the C-terminus of coil1b, missed the 17kDa band (Fig.1A, Suppl.Fig.1, Fig.2). This data indicates that stepwise and TBI-specific proteolysis produces the previously observed trauma induced GFAP-BDPs of 42, 37 and 18-25kDa[23]. Lastly, coil1-BDPs display greater coverage than coil2 BDPs (Fig.1B), an imbalance further supported by the significantly higher frequency of coil1 peptide presence compared to coil2 peptides which were consistently underrepresented across MS runs irrespective of sample or gel-slice (Suppl.Fig.3A, Method). Further, among detected peptides ion peaks indicated significantly greater coil1 than coil2 peptide abundance, providing added evidence on a biofluid imbalance between these two sets of BDPs controlling for patient and irrespective of gel-slice.

GFAP BDPs in Serum: We then immunoprecipitated GFAP from TBI patient sera and identified a coil1-product spanning S51 to R217 (97 residues, 18.2kDa, Suppl.Fig.4). With 59% sequence coverage, the termini could not be confidently identified. Noteworthy, coil2-containing peptides were missing in 4 different TBI blood samples, from 2 patients and one control (PrecisionMed).

In summary, exhaustive MS sequence analysis of GFAP in TBI patient biofluids revealed proteolytic processing that would be expected to generate equimolar co-products; however, coil1 products (20-23kDa) were more abundant and robustly detected than coil2 products (15-19kDa). This disparity was further confirmed by greater abundance of 20-23kDa bands versus 15-19kDa GFAP-BDPs in immunoblot densitometry of 24 TBI patients (Fig.8, see below). Notably, the detailed MS data indicate that GFAP degradation in TBI differs from that of other neurodegenerative diseases and cannot solely be predicted from recombinant GFAP digested with purified enzymes in cell-free systems or toxin treatments[34,52,53]. Additionally, we did not recover peptides spanning the region between coil1B and coil2B, suggesting the involvement of previously uncharacterized trauma-specific cleavage site(s). To address these unresolved issues, we next employed a trauma culture model using human primary cerebral astrocytes.

Human trauma model provides evidence of GFAP cleavage and reveals distinct distribution fates of coil1 and coil2 products.

Trauma generated GFAP co-products have different fates: The MS-based conclusions regarding coil1 and coil2 GFAP products were further investigated using monoclonal antibodies in a human trauma culture model[23,33]. Mechanical pressure-pulse stretching led to GFAP filament disassembly, release and degradation in traumatized astrocytes[23]. Immunoblots of cell lysates and concentrated culture medium of unstretched controls and stretched cultures from the same donors were probed using mAbs with defined epitopes (Fig.2; Suppl.Table 3). All clones detected full-length GFAP and large fragments, but differed in their detection of small BDPs (Figure 2)[54]. MCA-3E10, a coil1 marker, detected a 20kDa GFAP product in astrocyte medium that increased after trauma, but failed to detect it in cell lysates (Fig.2C, red). The more C-terminally targeted clone GA5 detected an epitope at the end of coil2 and the beginning of the “tail” sequence[35]. It detected a set of 17-28kDa GFAP-BDPs in cells but not in fluids (Figure 2C, purple). A cocktail of three monoclonal antibodies served as positive controls, revealing GFAP-BDPs in cells and fluids from the same donors (Fig.2C, blue). These experiments demonstrate that following mechanical trauma of human astrocytes, coil1 products were preferentially released, while coil2 products were selectively retained within cells. This provides new insight to explain the unequal presence of coil1/2 BDPs in trauma-released fluids.

Novel GFAP trauma cleavage is site defined by partial chemical breakdown of GFAP for mab5C10 epitope mapping: Clone MCA-5C10 detected full size and large GFAP fragments in cells and fluids after trauma. MCA-5C10 failed to bind any fragment smaller than ~40kDa, suggesting that it recognized an epitope that was destroyed in further trauma-associated GFAP proteolysis in both compartments when probed on the same donor samples as the other clones (Fig.2C yellow). MCA-5C10 showed weak but reproducible binding on dot blots to amino acids 233-261 of the human coil2A sequence (not shown). To pinpoint this clone's epitope further, a chemical-mediated partial digest of GFAP was used. The single tryptophan in GFAP, W256, lies within the region recognized by MCA-5C10. BNPS-skatole cleaves after tryptophan residue[29,30] to produce N-terminal 34.6kDa and C-terminal 20.5kDa fragments from recombinant human GFAP (Suppl.Fig.5). Clone MCA-5C10 bound avidly to this C-terminal fragment on western blots (Suppl.Fig.5). The identity of this 20.5kDa fragment was confirmed using the pan-intermediate filament antibody anti-IFA antibody to the C-terminal of coil2B (amino acids 358-377, ALDIEIATYRKLLEGEENRI) [31,32]. The MCA-3E10 antibody bound the N-terminal 34.6kDa band. We conclude that the sequence following the tryptophan: from tyrosine 257 to tyrosine 260, YRSKF, is an important component of the MCA-5C10 epitope, which likely also includes elements of the neighboring caspase 3 cleavage site, YRSKFA↓DLTD. Consistent with this, MS defined TBI-generated coil1 peptides extended no further than R239 with the N-terminus of coil2 products observed consistently at F261. This unique mapping data suggests novel trauma-cleavage(s) occur upstream of F261 combined with potential caspase 3 activity downstream of it.

Calpains and caspases cleave GFAP and show different astrocyte injury states.

Calpain and caspase inhibitors block trauma-activated GFAP proteolysis steps. The contributions of TBI-activated calpains and caspases to generating these TBI fragments was investigated with inhibitors of calpains and caspases[55-58]. AlphaII-spectrin breakdown products (SBDPs) served as positive controls with their common caspase and calpain indicator fragments, yet the protein's ubiquitous expression, (e.g., muscle, endothelial, epithelial and nucleated blood cells) limits its utility as a TBI biomarker[59-69]. Human traumatized astrocytes were treated with calpain inhibitor calpeptin, or with caspase inhibitor ZVAD-FMK, and GFAP-BDPs were analyzed in whole cell lysates, fluids and pelleted lifted cells and debris. αII-spectrin and SBDPs were abundantly expressed in differentiated human fetal astrocytes (Suppl.Fig.6), as reported in human gray and white matter astrocytes[70-72]. Both calpain (145/150kDa) and caspase (120kDa) SBDPs increased two days after stretch injury in cells, debris, and fluids and were decreased by their respective inhibitors (Suppl.Fig.6). Both, 145kDa and 150kDa calpain bands were observed in whole cell lysates, while the 150kDa showed in lifted cell pellets and 145kDa in culture fluids, respectively. The SBDP120kDa caspase indicator was enriched in the fraction of detached material and demised cells. This indicates that αII-spectrin calpain fragments, alike GFAP-BDPs, originated intracellularly, and also had distinct compartment preference after trauma, suggesting that selective distribution of specific cytoskeletal fragments was not unique to GFAP.

GFAP trauma proteolysis was analyzed from the same sample sets using MCA-3E10, a coil1 marker. Some GFAP appeared fragmented in unstretched viable cells due to baseline cytoskeleton turnover (Figure 3A) [73]. Two days post-stretching, all BDPs were elevated in cells, fluid and lifted material. Calpeptin reduced the 35-38kDa BDP and small BDPs while undigested GFAP initially accumulated in adherent cells and lifted material (Fig. 3A; Suppl.Fig.7). ZVAD-FMK inhibited the 19-26kDa small

BDPs effectively. Combined inhibitors (CV) had an additive effect, indicating that both calpains and caspases were involved in TBI-initiated GFAP degradation yet ZVAD-FMK is reported to also inhibit calpains[40]. Inhibitors reduced GFAP fragmentation in all three fractions. This data provides the first evidence of *endogenous* trauma-inflicted GFAP BDPs calpain and caspase activities going beyond non trauma experiments[53,74]. These findings connect traumatic GFAP proteolysis in human astrocytes with the well-known roles of calpains and caspases in TBI and cell death processes. The work supports the goal of using GFAP-BDPs as CNS-specific protease indicators after TBI[75,76].

Visualizing acute astrocyte injury states using live-cell protease reporters and membrane permeability. To begin identifying the cellular pathophysiology we imaged traumatized astrocytes using fluorescent calpain and caspase indicators together with the membrane wounding dye propidium iodide (PI). Cerebral in vitro differentiated astrocytes displayed two morphotypes: fibrous astrocytes with elongated processes and bushy-to-star-shaped astrocytes that resemble white and gray matter astrocyte morphologies[77] (Fig. 3). Under control conditions, both morphotypes displayed calpain activity (blue), but rare and low caspase activity (green). Fetal neocortical cells express calpains 1(μ) and 2(m) along with low endogenous calpain inhibitor calpastatin during the gestation times used here[78]. Five hrs post-stretching, injured astrocytes displayed blebbing with phase-dark vesicles and vacuoles and beaded processes, known as clasmatodendrosis (Figure 3B,C) [79,80]. PI-uptake revealed a mixed population of membrane-wounded astrocytes with varied PI-uptake that suggest dynamic membrane damage and resealing (Suppl.Fig.10). Phase-dense shrunken astrocytes with bright nuclear PI-stain lacked calpain or caspase activity indicating cell integrity loss that suggests acute necrosis. Membrane-damaged low-intensity PI-positive cells had variable caspase activity and either lacked calpain activity (elongated cells) or displayed active calpains and caspases (bushy cells, Fig.3B, Suppl.Fig.10). PI-positive caspase activity was associated with swollen cell bodies, vesicles and vacuoles. Caspase activity varied in cytosol and was strongest in nuclei, suggesting ongoing apoptosis.
Overall, preliminary imaging documents a range of parallel human astrocyte trauma phenotypes that are relevant to GFAP degradation after trauma. The findings suggest that distinct astrocyte subpopulations with different vulnerability and protease activities coexist soon after mechanical trauma. Endurance of traumatized astrocyte subpopulations, their integrity and enzymatic activity states warrant further studies.

Trauma generated citrullinated GFAP was uncoupled from regular GFAP, defining novel features in patient CSF and astrocyte proteinopathy.

Validated PTM mapping of TBI GFAP fragments: We analyzed mass spectra for TBI-associated PTMs such as acetylation and citrullination to identify TBI signatures crucial for a) biomarker assay development, and b) detecting cytoskeleton destabilizing proteinopathies that may impair astrocyte functions[81-86]. To our present knowledge, PTMs have not been characterized in human TBI patient samples, although GFAP citrullination was observed in chemically stressed cell lines, in cell-free reconstituted systems, and in the context of other neurodegenerative diseases[28,83,87]. Therefore, we validated the MS-detected acetylated and citrullinated peptide fragments by inspecting MS2 spectra for the presence of signature ions and neutral mass losses (see Methods). Validated were four citrullines in coil1 and three in coil2, including a potential novel citrullination site in coil1 (R79), which were consistent with observed mass deviations (neutral losses) in MS2 spectra (Fig.5A, Suppl.Fig.9;

Suppl.Table4). An additional five MS-detected citrullinations were previously reported to be citrullinated by PAD treatment in vitro[28]. The robustness of these MS-detected and validated citrullinations is supported by their repeated detection (Suppl.Table4).

TBI patients had different citrullinated GFAP signatures: Further evidence of citrullination was provided using citrullination-site-specific GFAP antibodies characterized in human traumatized astrocyte lysates (Suppl.Fig.10). Two antibodies to neoepitopes in citrullinated GFAP were selected and tested in nine CSF samples from five TBI patients in addition to the samples analyzed by MS (See Suppl.Table 3 and Methods) [36]. Citrullinated GFAP and fragments had patient-specific bands had distinct signal patterns that differed from that of unmodified, native GFAP signals detected in parallel (Fig.5B). Both citrullinated-GFAP antibodies robustly detected 13-16kDa and to a lesser extent, 26-30kDa BDPs that belonged, based on antibody epitopes, to coil2 products. Additional citrullination was detected among the large GFAP BDPs by CTGF-1221, with its epitope at R416. Additional citrullinated bands larger than 50kDa likely reflect GFAP bearing other PTMs (such as ubiquitination) or aggregated GFAP multimers[88,89]. Protease and deiminase activities occurred with patient-to-patient variability, documenting differences in GFAP modification and destabilization during TBI progression.

Citrullinated GFAP in human traumatized astrocytes labels non-filamentous aggregates: Citrullinated GFAP signals were investigated in traumatized and control human astrocytes combining cit270-GFAP, coil2-tail antibody GA5 and a polyclonal GFAP antibody (Figure 5). Traumatized cultures had more citrullinated GFAP than controls, both at 5 and 24hrs after stretch injury. Cit270 marked clusters of small speckles and large granules in a subgroup of astrocytes, but never appeared fibrous, as shown by GA5 and the polyclonal antibody (Fig. 5, Suppl.Fig.10). Aggregated and filamentous signals were generally not colocalized pending ultrastructural confirmation. Citrullinated GFAP either clustered in locally depleted GA5 regions or associated with exceptionally bright GFAP reported from disassembled GFAP in acutely wounded, calcium ionophore-treated, or calpain activated astrocytes[23,90]. Astrocyte morphotypes with cit-GFAP granules included reactive, atrophic (shrunken) and dystrophic astrocytes, named for swollen cell bodies and damaged or missing processes[91]. Cit270 signals were also detected as speckles peppered around astrocyte processes confirmed by phase-contrast images delineating astrocyte shapes (Suppl.Fig.10). Thus, traumatic injury-induced GFAP citrullination and filament breakdown was associated with aggregation and fluid release showing heterogeneity in astrocyte microstructures and patient CSF signals. Jointly, these findings provide new tools to study astrocyte degeneration using such pathological GFAP proteinopathies in connection with TBI biomarker signatures.

TBI patients' CSF profiles share acute GFAP peaks but have variable fragmentation patterns.

TBI trajectory of temporal GFAP degradation: Examples of the longitudinal GFAP heterogeneity is illustrated in two patients' sets of immunoblots with variable GFAP bands and signal intensities over consecutive CSF samples within two time windows (Fig.6A). Here, we measured full-lengths and GFAP fragments in CSF of 24 TBI patients collected from Neuro-ICU care (Suppl.Tables 1, 2) over 10 PIDs using recombinant 50kDa and 25kDa GFAP proteins for range-fitted calibration (Methods; Suppl.Fig.12). Each band was quantified by scaling various exposures expanding the dynamic range

from the lower limit of detection (0.027ng/ml CSF) to the upper limit of quantification (767ng/ml CSF; Suppl.Table5). GFAP proteoforms with similar profile and sizes were grouped, pooling migration variability within and across patients also seen in the MS data (Fig.1). GFAP trajectories had patient-specific peaks and troughs (Fig.7C-H) with acceptable variance spread (Suppl.Fig.12). Age had an effect on GFAP release and proteolysis with older patients showing higher CSF levels (Suppl.Table.6A, Suppl.Fig.14A). While this reflects known increases in GFAP biofluids in healthy elderly, age is also linked to altered clearance and worse TBI outcomes (see Discussion) [92,93]. Body temperature, concurrent with CSF draw, had a slight and significant effect on GFAP 45-49kDa fragments with smaller fragments in patients with fever (Suppl.Table 6B, Suppl.Fig.14B). Both covariate effects were included in the analysis model (see Methods). Total GFAP levels had an injury day peak that was 1.8SD units above the weighted mean[42] and displayed overall fewest extremes (p=0.035, Fig.6C). Full-length GFAP had the highest relative injury day peak with 2SDs above its weighted mean followed by decrease with lowest variability (p=0.012, Fig.6D). Mean levels of large GFAP fragments decreased sharply over first two PIDs, then remained flat around their overall mean (p=0.028; kurtosis: -1.3, Fig.6E). Mean levels of calpain-generated 37-39kDa fragments peaked with 1.5SDs above their overall mean, stayed elevated on PIDs 2-5 followed by a decrease during the second week (Fig.6F). Secondary rises were common among small BDPs 20-26kDa and their data had highest kurtosis (-1.8) and marked dispersion driven by both, sporadic peaks and undetectable values (interquartile range:3.18; variance: 2.8 log units). BDPs 15-19kDa peaked on injury day with 1.8 SD above their mean followed by secondary peaks and a more frequent non-detections than other BDPs (p=0.028; variance: 1.8 $\log(ng/ml)^2$, Fig.6H). Most bands' daily means exceeded the overall mean on until PID4 but fell below it from PID7 onward, highlighting a general decline over time. This result suggests that continued proteolysis of GFAP and its large fragments are associated with the temporary accumulation of smaller BDPs and an overall 10-day progressive clearance of GFAP in TBI CSF.

Fragment covariation and selective underrepresentation: We observed a strong correlation between the 50kDa GFAP and calpain-generated 37-39kDa fragments that suggests their co-release (Pearson coefficient, r=0.82, LogWorth=24.3; Fig.7A, B). The 40-42kDa fragments correlated also strongly with the 37-39kDa fragments indicating consecutive cleavage (r=0.73, LogWorth=16.3). The 15-19kDa BDPs related noticeably weaker with precursors 40-42kDa and 37-39kDa bands than 20-26kDa small BDPs (Fig.7; Suppl.Fig.14). Regarding the co-product sets, we noticed that their co-variance was weaker than expected considering they originated from same cleavage, based on MS and epitope mapping data done on a subset of this cohort. The 15–19 kDa BDPs had 28% greater absence than the 20–26 kDa BDPs across all 24 patients (Fig.7C). This co-product imbalance is consistent with less robust MS sequence coverage and lower aa detection frequency and signal peaks (Suppl.Fig.3). Thus, jointly these TBI patient findings support a selective astrocyte retaining of coil2 fragments and preferential coil1 product fluid release found in trauma cultures. Future work is warranted to investigate GFAP's in vivo fragment fates. Taken together, our findings suggest astrocyte-associated pathological coil2 aggregation co-occurs with fluid release of coil1 GFAP. These findings are consistent with the concept that both TBI pathologies initiate from the same cleavage event, yet coil-specific preferred fates could lead to differential compartment accumulation. This is translationally relevant, because linking any pathological cerebral protein aggregation, here GFAP proteinopathy with biomarker signals carries important implications for biomarker interpretation as

discussed later. Disrupted proteostasis -particularly cytoskeleton derangement- is an important part in TBI pathophysiology and neurodegeneration as we discuss below[94,95]. To begin addressing how GFAP, as a widely used biomarker, might be a proxy for overall injury burden, we have: (1) evaluated GFAP fragment levels under two severities in the trauma cultures and (2) evaluated GFAP BDPs in predicting TBI patients' outcome.

GFAP fragments inform on trauma severity and their early profiles predict TBI patient recovery

Time-sensitive calpain-specific GFAP-BDP release relates to trauma severity. The release of a 37kDa GFAP fragment was measured after 3psi versus 5psi pressure pulse stretching in 4-9 donor's astrocyte preparations from 0.5-48hrs postinjury and controls (Suppl.Fig.15). After severe stretch-injury, GFAP 37kDa fragments were elevated already at early timepoints (0.5-5hrs) over controls ($p<0.03$). Later postinjury (24-48hrs), these calpain-fragments were elevated in fluids of both severities ($p<0.001$). Their levels rose over time in both injury severities with differing kinetics (Suppl.Fig.15). This resulted in a severity of calpain-GFAP cleavage into 37kDa at 5hrs postinjury ($p=0.036$). Although further studies are warranted, these findings suggest that time-course of GFAP degradation besides their levels could become useful to evaluate trauma severity.

TBI outcome is predicted by levels of GFAP fragment trajectories not by those of full-length GFAP.
Proteolysis could relate to the underlying TBI patient burden following injury. To investigate how GFAP degradation related to patient recovery after TBI, we compared longitudinal CSF levels of full-length GFAP and its fragments in patients with favorable versus unfavorable six-month outcomes on the extended Glasgow Outcome Scale (GOSE). Age was included as joint covariate in the mixed model analysis (Methods). Adjusted CSF means of calpain-generated 37-39kDa GFAP BDPs differed with an effect size of 1.1 between patients with poor recovery (GOSE 1-4) and those with favorable outcomes (GOSE 5-8, $p=0.02$; Fig.8, Suppl.Table7). Small 20-26kDa BDPs separated good-versus-poor GOSE early postinjury and during the second week, while adjusted means overlapped 3-7PIDs due to frequent undetected values (Fig.8B). Full-length GFAP levels and their adjusted means substantially overlapped during 10PIDs. Similar outcome predictions for same GFAP proteoforms were observed using stricter favorable outcome (GOSE7+8), indicating the findings did not depend on dichotomization (not shown). In summary, longitudinal profiling of GFAP degradation products offers greater prognostic resolution than full-length GFAP alone, and hence may support early risk stratification and outcome prediction in TBI patients.

In conclusion, TBI triggers coordinated and specific GFAP destabilization via citrullination, other PTMs and stepwise proteolysis that is associated with astroglial integrity lapses and astrodegeneration. Pathological GFAP aggregation and fragment-specific biofluid profiles are interrelated as co-products generated by same TBI-GFAP cleavages and thus offer monitoring of evolving TBI pathophysiology and recovery.

Limitations: The clinical study had limited patient sample collection, as it was conducted during the Covid pandemic under substantially short-staffed Neuro-Intensive Care unit personnel. Large cohort studies are needed for further covariate inclusion, yet within the cohort, same GFAP band-signals were measured in all 102 samples using subsaturated, calibrated, and scaled raw data. The

longitudinal profiling was truncated at 10 PIDs to avoid violating unequal variances. The remaining sample size used omega squared to compute age and temperature effects. Cohen's D effect size was used to predict good versus poor outcomes, as area-under-the-curve accuracy testing was inadequate for simultaneously including elapsed time postinjury. MS sequencing was done using TBI CSF and only limited serum. Ventriculostomy for CSF drainage is employed in 45–80% of severe TBI offering unique biomarker insights for TBI monitoring while carrying a small risk of infections [96,97]. UCLA surgical pathology procurement of donated fetal brain specimen allowed setup of cerebral astrocyte cultures[23,33], yet primary tissue amounts are limited to cover all relevant conditions simultaneously to address coil1 & 2 fragments, key timepoints, controls and severity settings for various protease inhibitors. Shown data was pooled from six cultures and was representative for other donors. Live-cell staining limited the use of high-intensity or repeated fluorescence imaging but enabled simultaneous monitoring of both enzymes and membrane permeability at a single timepoint. This approach provided insight into coexisting astrocyte injury states, as well as GFAP degradation, modification, and distribution, offering relevant information on astrodegeneration and TBI monitoring.

Discussion

This study describes novel TBI-induced GFAP degradation products and proteoforms and demonstrates trends over time with unique patient-specific profiles. GFAP proteolysis and release are progressive processes while distinct cerebral astrocyte injury states may coexist. We highlight a novel TBI cleavage that produces two sets of products with distinct distribution fates from a common fragment precursor. Specific GFAP BDPs have clinical significance for pathophysiology, longitudinal monitoring, and predicting outcome. These findings are novel and inform on the complexity of astrodegeneration that could advance our understanding of pathomechanisms during the subacute setting after TBI.

With this use-context in mind, interpreting biofluid GFAP signals is desired. Assaying of biofluids after TBI is now frequently used for acute brain injury using commercial antibody-based assays. Beyond a general specificity for GFAP it is not clear what proteoforms are being measured, as this information is either proprietary or unknown[10,14,98]. Yet it is presumed that total trauma-released GFAP is being captured. We used MS and domain-specific and modification-selective antibodies to identify TBI-induced GFAP proteoforms, their profiles and distribution after trauma. This study informs that coil1 and coil2D products exhibit distinct release patterns, crucial knowledge for designing sensitive and specific assays. Underlying perturbed proteostasis with pathological citrullinated coil2-fragment aggregation after injury is documented. Together, our findings provide an important first step toward understanding how GFAP proteoforms that reflect pathological processes following TBI.

Cellular and biochemical pathophysiology of mechanical force induced traumatic injury. Mechanical trauma or whiplash shear brain tissue, causing diffuse axonal injury and astroglial clasmatodendrosis -membrane wounding that can lead to protracted cell loss[23,79,99-101]. Trauma ruptures plasma membranes via mechanoporation, causing rapid initial protein release[102,103] -

including full-length GFAP and large fragments- followed by later generation and release of small GFAP-BDPs linked to astroglial death[23]. Mechanical forces also stretch and can break intermediate filaments that may initiate protein aggregation[104,105]. Under biomechanical high-speed strain, filaments get stretched, disassemble exposing the rod center making it vulnerable to proteases[73,90,106] or may reach a molecular breaking point[105,107]. Indeed, non-filamentous GFAP has been documented minutes after stretch-injury in mechanoporated human astrocytes[23]. Thus, filament-disassembly is closely linked to membrane permeability perturbing ion balance that threatens cell viability[23]. Ion dysregulation is followed by water leading to membrane blebbing and astrocyte swelling (oncosis). If unresolved, and with energy resources being depleted cell integrity maybe lost resulting in necrosis. Burden from reactive oxygen species, acidosis and hypoxia further impair mitochondria eventually shifting from apoptosis to necrosis[108-113]. This progressive pathophysiology may occur in human astrocytes with considerable delay (unpublished comparison of human and rodent astrocytes) and could contribute to secondary GFAP release in TBI patients reflecting cytotoxic edema and subacute astrocyte loss[114-119].

Linking proteases and destabilizing enzymes to GFAP proteinopathy and astrocyte pathology. Treating rat astrocytes with a calcium ionophore causes rapid and transient increase in cellular GFAP immunocytochemical signals due to filament unwinding that exposes additional epitopes[90]. As aforementioned, trauma-induced unwinding can also reveal a concealed proteolytic cleavage site in the rod center of GFAP. Calcium augments GFAP proteolysis, rapidly activating *calpain* through a conformation change leading to initial partial GFAP cleavage, consistent with calpains' limited proteolytic activity[73,90,103,120-128]. Calpains and caspases both participate in GFAP proteolysis in stretch-injured astrocytes as calpain cleavage activates caspases[125,129]. Our observation of unstretched calpain activity is consistent with calpains being part of the ubiquitin-proteasome, autophagy-lysosomes, and cytoskeleton remodeling systems, active at baseline and regulated by endogenous inhibitors such as calpastatin[78,130-132]. Our live imaging documents coexisting astrocyte injury states with active calpain and caspases, indicating that various progressed states of astroglial wounding coexist due to astrocyte subtype differences, bushy versus fibrous morphotypes, or variations in focal mechanical loading and cellular energy exhaustion. Active *caspase* activity in process-damaged and blebbing human astrocytes after trauma parallels early post-lesion caspase activity seen in clasmatodendrotic rat astrocytes following excitotoxicity, linking cytoskeleton remodeling, its caspase-mediated breakdown, and apoptosis[123,133,134]. Variability in membrane damage and energy depletion shape cell resilience and produce a spectrum of concurrent cell injuries[101,118,135]. These pathological GFAP changes impair astrocyte function, risk diminished glutamate buffering and neuronal support that could lead to neurodegeneration[136]. Calcium also activates peptidylarginine deiminases (PADs) among other enzymes that destabilize cytoskeleton proteins including GFAP by *citrullination* leading to proteinopathies in neurodegenerative diseases such as Alexander disease[81-86,137]. We show TBI patients with such GFAP destabilizing proteoforms. In our trauma model stretch-injury drives pathological GFAP aggregation in human astrocytes consistent with GFAP citrullination after mechanical stretching, hypoxia and chemical injury that upregulate and activate PADs in other culture models of rat and human astrocytes and Müller glia[88,138,139]. Assembled GFAP filaments are vital for maintaining astrocyte morphology, mechanical resilience, ATP release and other essential functions[73]. Thus, the *GFAP proteinopathy* shown in our study signifies *pathological astrocytes* with potential harmful consequences that, as seen in

Alexander disease, critically impair astrocyte function, jeopardizing neural metabolism, network activity and the integrity of the neurovascular unit[140,141].

Trauma caused GFAP fragment sequences. TBI patient GFAP BDP sequences show novel cleavage patterns, distinct from established protease sites in other neurodegenerative diseases. A caspase 6 cleavage of GFAP ($VELD_{225}$-VAKP) was described in mouse culture models of Alexander disease, splitting GFAP at the linker2 sequence, with the C-terminal coil2 fragment detected by antibody GA5 [34,35]. The present study identified TBI patient-defined coil1 products with ending sequences that repeatedly contained an additional 8 or 14 amino acids that are distinct from the cleavage seen in Alexander disease [34]. Hence, we conclude that a new proteolytic cleavage occurred between residues 240-260 after TBI that produced these trauma-related GFAP-BDPs.

The TBI patient coil2 products we identified begin at F261 and end at R390 or K410, making them shorter than the GFAP 20kDa and 30kDa fragment pair reported in Alzheimer's disease patients generated by caspase 3 cleavage at $_{258}$RSKFA↓DLTD in coil2A[52]. This cleavage does not explain the shorter coil1 or coil2B fragments we detected; rather, our findings point to coil2B being particularly sensitive to proteolysis. Our data implicate calpain and caspases in this process, though other proteases -including possible endogenous trypsin-like activity (YRSK↓F_{261})- may contribute. Such activity could generate the new termini found in both TBI-GFAP small products (LTAALKEIR↓T; R239) that would account for the observed sequence gap between them. Endogenous trypsin activity has been reported after brain injury inflicting astrocyte compromise and adverse inflammatory effects[142,143]. Our rigorous MS high confidence peptide maps and MCA5C10 epitope loss ($_{257}$YRSKF_{261}) flanks a neighboring caspase 3 cleavage site. The gap between the two co-products was unlikely an experimental artifact, as high confidence peptides were detected repeatedly covering that region during MS runs of longer GFAP precursor fragments and recombinant GFAP sequencing. Further studies are needed to delineate all proteases involved in GFAP cleavage after TBI. The variability in fragment presence and termini suggest different enzymes and fragments could reflect different TBI phenotypes and astrocyte injury populations.

Structural evidence for protease vulnerability of the novel TBI cleavage site. Intact GFAP molecules anneal by α-helical coiled-coil interactions forming parallel dimers, antiparallel tetramers and ultimately 10nmØ units that grow in length to mature filaments[54]. Computer modeling and structural data show that the entire rod segment of vimentin, closely related to GFAP, is a continuous α-helix[144]. This is despite several regions, historically referred to as linkers or stutters, lack the typical hydrophobic heptad repeat pattern of α-helical coiled-coils. These regions contain proline and other turn-promoting aa or feature 11aa (hendecad) sequences disrupting the heptad repeats. These regions were therefore thought to represent non-helical linkers. Notably, the Alexander disease-associated cleavage site discussed above is found within one such non-helical "linker12", consisting of several hendecad repeats. Likewise, the region containing the MCA5C10 epitope and caspase3 site were historically referred to as "stutter1", where a hydrophobic heptad repeat (7aa) is replaced by a single hendecad sequence, disrupting the packing and thereby can render both regions more susceptible to proteases[145].

Novel GFAP co-product patterns-pathophysiological significance and biomarker implications. TBI proteolysis of GFAP generates co-products with unequal MS sequence coverage, peptide frequency and abundance in patient biofluids. MS disparities reflect coil1-BDPs to be more prevalent

than coil2-BDPs in TBI CSF, while the later were undetected in serum. GFAP concentrations are generally lower in blood versus CSF due differences in dilution solute passage between the interstitial space and ventricles, versus capillaries and blood vessels[146-148]. Immunoblotting with a polycloncal antibody also shows an imbalance with of 20-26kDa BDPs over less abundant less frequent 15-19kDa BDPs in 24 TBI patients, paralleling MS data. The imbalance could reflect differences in release or susceptibility to further degradation. While we do not have data on GFAP fragment-specific clearance, stretch-injured astrocytes show preferred coil1-BDP trauma-release and selective coil2 BDP retention using coil-specific mabs. Traumatized astrocyte retention and modification of coil2-BDPs as non-filamentous GFAP aggregates mirrors Alexander disease, where mutant GFAP fragments disrupt proteostasis, form toxic Rosenthal fibers that impair astrocyte function driving neurodegeneration[34,35,136,149-151]. Thus, traumatized astrocytes with cit-GFAP aggregates are a) a signature for *astrocytopathy* and b) are linkable to GFAP in TBI biofluids. TBI CSF samples carry both co-products. However, coil2-BDP signals varied -were either missing or elevated- possibly indicating presence or absence of a pathological event leading to *integrity loss* with release of otherwise retained proteoforms. Astroglial membrane lysis from necrosis or oncosis during cytotoxic edema may account for such release (see below). Coil-specific and citrullinated GFAP antibodies may aid assay development for detecting astrocyte-driven TBI pathologies[80,152,153]. On one hand, coil1-GFAP fluid maybe matched by a latent coil2-GFAP burden in the injured brain. On the other hand, detecting coil2 in fluids may signal worsening conditions such as cytotoxic edema with unregulated astrocyte demise. These possibilities highlight two priorities for future research of present needs: (1) examine cit-GFAP-aggregates in postmortem TBI, BLAST, or CTE brains to establish traumatic astrocytopathy as new TBI neuropathological hallmark with modified GFAP proteoform antibodies; and (2) linking GFAP biofluid elevation to proteostasis disruption and neurodegeneration in animal TBI models[95,154]. Overall, our findings offer connecting GFAP as a TBI fluid biomarker with ongoing proteinopathy and may aid to explain recurring GFAP elevations due to secondary deterioration observed in TBI patients[21,23].

Potential clinical impact for new GFAP 'context of use' in neurocritical care TBI monitoring.
Possible new COUs for GFAP in TBI patient assessment warrant discussion: *(1) Longitudinal monitoring*; (*2) Contusion expansion through cytotoxicity and (3) Outcome prediction*.
(1) Longitudinal TBI monitoring: GFAP degradation kinetics offer a valuable longitudinal window for Neuro-ICU TBI patient monitoring during intensive care and early clinical trial endpoints[57,155-162]. In circulation GFAP-BDPs dominate, while CSF also contains both, uncleaved GFAP alongside BDPs[23,163,164]. Temporal biomarker profiles show that all GFAP forms typically peak on injury day, a pattern shared with a subset of other cytosolic and cytoskeletal proteins (e.g. UCH-L1, S100β, aldolase C, neuron-specific enolase, αII-spectrin). Early peaks reflect acute mechanoporation, force-triggered filament breakage and calcium-driven proteolysis[23,24,63,102,165,166]. Hence, calpain-generated 37-39kDa GFAP BDPs correlated strongly with full-length GFAP supporting common origin in TBI CSF.
After initial trauma small BDPs occasionally display secondary rises (4-5; 9PIDs), reflecting caspase activation in some patients. This pattern aligns with secondary serum GFAP peaks (4PIDs) in a subset of older TBI patients with high CT burden, poor outcome, high mortality and pathophysiological features of more severe TBI patients[21]. We observed higher GFAP CSF levels among older patients as well. Age-related increases in baseline GFAP and neurofilament light (NfL) relate reduced clearance or ongoing parenchymal atrophy[92,93,167-169]. Elderly suffering a TBI clear CSF less efficiently through

decreased CSF pulsation, ependymal cilia vulnerability, and disrupted cerebral blood flow, further elevating biomarker levels[170-172]. Finally, secondary GFAP-BDP spikes exhibit vary between patients, reflecting heterogeneity in secondary in secondary injury progression.

(2) Longitudinal GFAP-BDP profiles due to progressive astrocyte pathology may inform on secondary injury. Neuroimaging finds expanding contusions after TBI affecting peri-lesional tissue with one underlying pathomechanism being cytotoxic edema[173-177]. Cumulative astrocyte swelling, secondary membrane integrity compromise, and loss underpin such microstructural changes driven at large by ion dysregulation and metabolic imbalance[114-116]. Ongoing injury events like these contribute to TBI patient heterogeneity that is also reflected in varying GFAP-BDP trajectories we report. Progressive astrodegeneration is quantified in autopsied brain tissues of TBI patients documented by reduced astrocyte numbers between acute (<6h) and subacute (>6hrs to 3PID) postmortem timepoints in cerebral white matter and hippocampus[119]. Accordingly, GFAP-BDP profiling in the Neuro-ICU may be considered as a tool to monitor secondary adverse postinjury events. An expanded window of biofluid testing in neurocritical care may aid individualized insights into an evolving pathophysiology, beyond single-timepoint GFAP testing in the emergency department.

(3) Temporal GFAP-BDP trajectories predict TBI patient outcome. Elevated GFAP in CSF and blood is well-documented as prognostic marker for severe TBI recovery[21,23,178-181]. Our longitudinal study further specified that among GFAP proteoforms, trauma-generated calpain GFAP-BDPs (37–39 kDa) differentiated poor versus good 6-months outcome, regardless of how recovery scores were dichotomized. This is important as evaluating "good" recovery is a very personal determination[182]. Profiles of small BPDs (20–26 kDa) followed this trend. In contrast, uncleaved GFAP levels failed to predict recovery. Jointly, our data emphasize that *ongoing pathological proteolysis* could inform on injury progression and recovery rather than merely the level of GFAP *release* as such. Current FDA-approved GFAP assays focus on a narrow injury-day window[9,178] missing this dynamic. While GFAP assays may include detecting BDPs, they don't differentiate GFAP fragments and longitudinal detection is presently not part of the COU. Thus, collectively, while uncleaved GFAP release, conceivably from initial trauma, is less indicative of injury course and prognosis, monitoring GFAP-BDPs post-TBI have the potential to improve predicting mortality and functional outcomes[183], as magnitude and trajectory of GFAP proteolysis are shaped by the evolving burden of brain injury that may drive recovery.

In summary, this study delineates the stepwise proteolytic processing of GFAP following TBI, highlighting the distinct molecular signatures and PTMs that underpin astrocyte dysfunction and neurodegeneration. The identification of trauma-specific GFAP BDPs, their divergent fates, and the mechanistic link to both acute biomarker release and latent proteinopathy provide a novel foundational concept for improved TBI phenotyping and patient monitoring. These findings underscore the importance of assay design tailored to GFAP proteoform heterogeneity and support the use of longitudinal GFAP-BDP trajectories as robust neurocritical care predictors of progressing injury course and clinical outcome.

Data Availability:

The data masterlist comprised of de-identified TBI patient clinical variables and outomes, CSF collection and all GFAP band-specific measurements of the DANA study cohort are uploaded to the Open Data Commons for Traumatic Brain Injury, Wanner lab and is accessible on ODC-TBI with Data dictionary here:

https://odc-tbi.org/lab/dataset?labid=387&datasetid=1432

Authorship Contributions:

IBW conceptualized and designed the study, wrote and revised the manuscript, curated data and conducted formal analysis, designed and prepared all visualizations, acquired funding, coordinated research activities, supervised laboratory assistants and students and conducted cell culture and live cell imaging studies. **JH** and **JL** conducted sample preparation and immunological experiments, assembled raw data and illustrations, curated and analyzed data. **JL, SS** and **YC** analyzed MS spectra. **YC** and **SS** conducted MS analyses. **HZ** provided the thumbnail infographic. **CS** analyzed data and provided visualizations. **ROL** and **JAL** provided MS data analysis guidance and **JAL** was involved in the study conceptualization. **TVM** and **GS** provided antibodies, peptides and recombinant proteins and offered biochemical guidance. **GS** also conducted antibody binding and chemical cleavage studies and wrote the structural part of the discussion. **BME** conducted clinical MRI and on TBI patients and provided data interpretation. **JG** provided guidance on data curation and statistical analysis approaches. **SR** and **PMV** had oversight over clinical aspects of the study including TBI patient enrollment, IRB approval and sample provision, further, **PMV** provided guidance on clinical interpretation of the findings. Resources included **IDDRC** laboratory infrastructure including cell culture, centrifuges, gel imagers. The **MIC** provided mass spectrometry instruments and proteomics facilities for the study. ***All authors*** *read, reviewed, edited and approved of the manuscript*.

Acknowledgements

The authors acknowledge with appreciation the receipt of mouse antibody CTGF-1221 to citrullinated GFAP (RRID: AB_3678889) that was kindly provided by Dr. Akihito Ishigami, Tokyo Metropolitan Institute of Gerontology, Tokyo, Japan. Special thanks goes to Dr. Sarah Dry and Ko Kiehle Translational Pathology Core lab, Ronald Reagan UCLA Medical Center, and Dr. Angela Chen, Family Planning & UCLA OBGYN Ronald Reagan Medical Center, for consenting and procuring voluntary donated fetal remains as pre-shelved specimen for cerebral tissues. Greatly appreciates for their grateful for input from are Laboratory assistant Kiohei Itamura, and UCLA Honors students Michelle Gong, Raghu Padmanabhuni, Aryana Sargsyan, Ana Karimi Bidhendi, Emerald Wong, Mhina Cham, Aryana Sargsyan, Kunal Ranat; David Sanville, and for the valuable critical care management assistance provided by Courtney Real and Jesus Ruiz-Tejada and the help from clinical fellow Azim Laiwalla.

Competing Interest:

IBW and **JAL** are inventors of the following patents licensed to BRAINBox Solutions Inc., where **TVM** serves as Chief Scientific Officer (CSO). **GS** is CEO and founder of EnCor Biotechnology Inc., which distributes several monoclonal GFAP antibodies used in this study.
US Patent Issue No.: US 10,557,859 B2 original patent; Inventors I.B. Wanner and J.A. Loo, Issue date: 2/11/2020; 25 claims prior publication 12/20/2018: Astrocyte traumatome and neurotrauma biomarkers. Applicant Regents of the University of California, Oakland, CA. Licensee: BRAINBox Solutions Inc.
US Issue No.: US 11,249,094 B2 Additional 13 claims in divisional patent 13 Claims, Filed 12/116/2019; Issue date: 2/15/2022; Inventors: Wanner and Loo, UCLA: Astrocyte traumatome and neurotrauma biomarkers. Assignee UCLA; Licensee: Brain Box Solutions Inc.

Funding:

Dana Foundation: Clinical Neuroscience “First in man” award # 20182601
Brain Injury Research Center (BIRC), State of California
NIH/NINDS Small Business Innovation Research, SBIR grant # 1R43NS106972-01
Semel Institute IDDRC and Brain Injury Research Center, BIRC, UCLA, Los Angeles, CA, USA
Sponsored Research Agreement, Abbott Diagnostics
Sponsored Research Agreement, BrainBox Solutions Inc., Richmond VA, USA

Figure Legends

Thumbnail: Astrocyte injury states with GFAP proteoforms and fates after TBI
The infographic depicts four distinct, progressive -and partially coexisting- pathophysiological states of human astrocytes following TBI. Each injury state is characterized by specific cellular morphologies and GFAP proteoforms and their molecular fates. Illustrated are key processes of GFAP degradation and proteinopathy together with ensuing astrocyte dysfunction that jointly offer a mechanistic basis for longitudinal GFAP fluid biomarker signatures. Understanding these astrocytic and cytoskeletal alterations is central to interpreting GFAP as a TBI biomarker and linking it to neurodegeneration. The thumbnail captures the reasoning for a new GFAP TBI COU in Neuro-ICU patient monitoring and recovery prognostication. **(1) Uninjured***, healthy* astrocyte: Intact processes, continuous plasma membrane and fully assembled GFAP filaments. **(2) Mechanoporated***, wounded* astrocyte: Shear-forces and mechanical loading inflict membrane damage, poration and process beading (clasmatodendrosis), triggering calcium influx and ion imbalance. GFAP filaments get stretched and disassemble into GFAP monomers that may even break (black) and are subsequently degraded, initially by calpains into large fragments (gray BDPs), followed by calpain, caspase and other proteases into novel TBI cleavage co-products: sets of coil1-BDPs (red) and coil2-BDPs (purple). Coil1-BDPs are released into fluids through permeable membranes (red), while coil2-BDPs form intracellular aggregates (purple clusters). **(3) Dystrophic (oncotic),** astrocyte: *Swollen* with vacuoles, membrane blebbing and advanced process damage. Accumulated PTM-modified GFAP granules marked by citrullination (green) and acetylation (brown) represent a GFAP proteinopathy newly recognized in TBI. **(4) Necrotic,** *dying* astrocyte: Loss of membrane integrity, membrane rupture and uncontrolled lysis release modified GFAP aggregates associated with astrocyte demise.

Figure 1: TBI patients' GFAP-BDP sequences display variable product endings.
A) TBI patient CSF immunoblots of a 15% gel show GFAP detected by a polyclonal (top) and a monoclonal (clone 3E10, bottom) antibody (postinjury days, i+1 through 1+3) of an 84 year old male sustaining facial fractures, subarachnoid and intraventricular hemorrhage and intraparenchymal hematomas from a fall. Observed GFAP band molecular weights were bands (II.) 36-39kDa, bands (III.) 20.4-23kDa, and bands (IV.) 17-19kDa, missed by clone 3E10. **B)** MS peptide maps of immunoprecipitated GFAP breakdown products (BDPs) of four cut out gel bandsets (I.-IV., Suppl. Fig. 1) from six CSF TBI samples of three patients. Percent of fragment sequence coverage (left) by high confidence (green, FDR≤1%) and repeatedly identified medium confidence (yellow FDR≤5%) peptides. Bands (I.) had 359 amino acids (aa) with calculated molecular weight of 41.7kDa and suggested new N- and C-termini of serine 53 (S53) and lysine 411 (K411). Bands (II.) spanned 349 aa from glycine 56 (G56) to leucine (L404) within which 37/38kDa fragments with variable endings between TBI samples were located (Suppl Fig.1). Bands (III.) contained two GFAP BDPs, 92% covered coil1-containing product of 185 aa, calculated molecular weight of 21.8kDa; 77% covered coil2-containing product of 151 aa and peptides, estimated molecular weight of 17.5kDa. Bands (IV.) 96% covered 181 aa coil1 product with size between 21-21.6kDa -±PTMs; and 77% covered coil2 product of 130 aa with estimated molecular weight of 15-15.3kDa.

C) Predicted endings of the two sets of novel TBI patients' GFAP-BDPs. Coil1 products N-termini were S53 (III.) and alanine, A55 (IV.) and new C-termini were arginine 239 (R239) C-terminus (III.) and A233 (IV.), both stretching beyond previously described caspase 6 cleavage around VELD225[34]. Coil 2 products had consistent N-terminus phenylalanine 261 (F261), see reported caspase 3 cleavage RSKFA↓DLTS[52], and variably ended with K411 (III.) and with R390 (IV.).

Figure 2: Novel GFAP cleavage creates co-products with distinct localization fates in TBI.
Monoclonal antibody (mab) mapping confirms GFAP cleavage into two co-product sets that resided in separate compartments using a human trauma culture model of in vitro differentiated cerebral astrocytes[33]: coil1-containing products were trauma-released and coil2-products remained cell-associated. **A)** Coil1 or coil2 harboring small GFAP-BDPs for antibody epitope alignment.
B) Binding regions and defined epitopes of GFAP mabs within coil1 and coil2 GFAP-BDPs. Mab 3E10 binding region is in coil1B between aa 196-217 with stutter motif HEEEVRE, aa204-210, as epitope. Binding region of mab 5C10 covers aa 240-260 in coil 2A with aa257-260 as core epitope. Mab GA5[34] binds at the end of coil 2B covering aa 374-390. Mouse GFAP multiclone antibody (4A11, 1B4, 2E1 BD Pharmingen) contains unspecified epitopes in both coils. **C)** Two donor's whole cell lysates (Cells) and concentrated media (Fluid) from control (-) and 2 days post-stretched human astrocyte cultures ("+", 4.8-5.4psi) were probed with mab GFAP antibodies. All clones detected full-length GFAP and large fragments in cells and trauma-released fluids. Mab 3E10 detected 20kDa products in fluids missed small BDPs in cells. BD Multiclone detected 13-28kDa GFAP BDPs in cells and fluids. Mab 5C10 did not detect small fragments. Mab GA5[34] detected 17-28kDa GFAP BDPs in cells, missed small BDPs in fluid.

Figure 3: Inhibition of trauma-induced GFAP degradation across compartments and live imaging of astrocyte injury states show calpain/caspase activation and cell integrity compromises.
A) Unstretched or stretch-injured human astrocytes were treated with calpain inhibitor calpeptin (C, 13mM), caspase inhibitor Z-VAD-FMK (V, 11mM), both (CV), or no drug (-) for 48 hours. Adherent cells were lysed (Whole Cell lysate, WCL), centrifuged fluid pellet contained lifted material (Lifted Cell Pellet) and fluids were concentrated (Conditioned medium, CM). *Top:* 2sec exposures for 50kDa GFAP and 42-47kDa BDPs. *Mid:* 1min exposures for 38-25kDa BDP bands. *Bottom:* 20min (WCL, CM) and 5min (Lifted cell pellet) exposures for 17-25kDa BDPs (See Suppl.Fig.7 for 5hr blot and 48h densitometry). **B+C)** *Live imaging of distinct cerebral human astrocyte morphotypes and their acute trauma stages defined by membrane leak, calpain and caspase activities during 5-6 hours postinjury.* **B)**. *Left*: Elongated (*Top*) and bushy (*bottom*) morphotypes and injury shapes on phase contrast. *Right*: Fluorescence images for plasma membrane permeability (5min uptake assay of propidium iodide, [PI+], red), calpain activity (CMAC-tBOC-leucyl-methionine, [CMAC-tBLM], converted substrate, blue) and caspase activity ([NucView488] converted substrate, green). *Top*: Control fibrous astrocytes display intact processes, acutely stretched cells had thinned, frequently beaded clasmatodendrotic processes (arrows). [PI-] astrocytes were calpain active. [PI+], leaky cells presented variable caspase activity (yellow/orange), lacking calpain-activity. *Bottom*: Bushy control and stretched astrocytes were calpain active (blue). The majority of stretched bushy astrocytes were calpain and caspase active (teal). [PI+], leaky bushy cells either retained both activities

(yellow/white), or lost these protease activities (red, arrows) displaying necrotic, atrophic morphology. Phase-dense vacuoles were unstained.
C) Enlarged from B: Individual fibrous (top) and bushy (bottom) astrocytes showing distinct structural and functional features of intact, injured and necrotic astrocyte phenotypes: *Intact* [PI-], calpain[+]; *Wounded*: [PI-/+], cytoplasmic and nuclear caspase[+]; *Dying:* [PI+] nuclear caspase [-/+], calpain[-]. Suppl.Fig.8 for separate fluorescence channels). Scale bars: 100 µm.

Figure 4: Destabilizing citrullination and acetylation PTMs are signatures of TBI patients' GFAP.
A) Map shows GFAP coil1/2 BDPs with posttranslational modified aminoacids from MS of 6 TBI CSF samples. Citrullinations (green) included a novel citrullination site at arginine 188 (R188), and acetylations (brown) PTMs were validated by signature ions and ion mass shifts in MS2 spectra (Suppl. Figure 6). *Here identified citrullinations are prior described in cell-free peptidylarginine deiminase digests[28]. Arrows: Neo-epitopes R270 and R416 for citrullinated-GFAP specific antibodies cit-R270-GFAP, mab CTGF-1221[36] used in B and Fig.5. **B)** *Left*: TBI patient-specific citrullinated GFAP-BDP signatures in nine CSF samples from five TBI patients using two citrullinated-GFAP antibodies. Besides fragments, larger modified GFAP bands were present. *Right*: Unmodified GFAP detected by cloil1 mab3E10 (top) or a rabbit polyclonal GFAP (bottom) show different signal patterns and amounts as citrullinated GFAP on same samples (dilutions and exposures given below blots, antibodies see Suppl.Table3).

Figure 5: Trauma induced citrullinated GFAP formed aggregated clusters in pathological human astrocytes
A) Immunofluorescence of coil2 GFAP (mabGA5,red) and citrullinted GFAP (cit270-GFAP, green) shows trauma-enhanced accumulation of non-filamentous citrullinated GFAP clusters at 5 and 24 hours post-stretching (right) versus control astrocytes (left) astrocytes. **B)** Unstretched astrocyte (left) and three trauma-pathological astrocyte morphotypes (right) after stretch-injury: reactive astrocyte with thick, hypertrophied processes and bright GFAP with somatic fine-granular cit-GFAP (yellow); astrocytes with fanning-out processes display cit-GFAP sprinkles around GA5 signals (arrows); dystrophic, oncotic astrocytes with swollen somata and malformed or missing processes display non-filamentous GFAP and cit-GFAP aggregates (arrowheads; Suppl.Fig.10E, and polyclonal GFAP signals, F for cell borders. Scale bars: 50 µm.

Figure 6: TBI patient longitudinal CSF GFAP size-specific patterns display common acute GFAP peaks, individual secondary GFAP profiles and unique GFAP degradation profiles.
A) GFAP immunoblot of 16 serial CSF samples over four postinjury days from a 40 year old white male TBI patients with admission GCS 3 and good recovery (GOSE score 8). Strongest GFAP and fragment signals were six hours postinjury and secondary peaks of GFAP (37-50kDa) occurred on PID two, three and four. **B)** GFAP immunoblot shows seven serial CSF samples from PID4-10 of a 48 year old Hispanic male TBI patient with admission GCS10 and GOSE6 outcome. Bands 37-50kDa were stronger on earlier days while 15-26kDa BDPs variably increased on PID5-8. **C-H:** *TBI patients' 10 PID longitudinal profiles of GFAP total* ***(C),*** *uncleaved* ***(D)*** *and degradation BDP sets* ***(E-H).*** Graphed are log-transformed GFAP CSF trajectories measured on repeated exposures of subsaturated scaled and calibrated (colored lines; 102 observations, 24 TBI patients; densitometry approach see

Suppl.Fig.11; Suppl.Table5). Added are estimated resampled mean cubic splines with 95% confidence bounds, interquartile range (IQR, log ng/ml), kurtosis and variance (σ: log(ng/ml)^2).
D, E, H) Total, full-length GFAP and 15-19kDa BDPs were significantly higher on injury day than on other PIDs ($p<0.05$; Linear mixed model, controlling body temperature and age, Suppl.Table6, Suppl.Fig.13). 15-19kDa BDPs had large dispersion due to high or undetected bands (difference to other proteoforms see I, K). **F)** Calpain-generated 37-39kDa GFAP fragments trended high on injury day ($p=0.06$) and displayed above mean signals until PID3, around mean signals on PID4 and 5 and below mean signals thereafter. **G)** Small GFAP BDPs sized 20-26kDa had pronounced secondary highs and largest dispersion (highest IQR, variance and kurtosis).

Figure 7: Correlation between sets of GFAP proteoforms in TBI patients' CSF.
A) Multivariate Pearson's correlation matrix shows correlation coefficients between uncleaved GFAP and all BDP sets measured in same TBI CSF samples. **B)** Bivariate graph of full length (50kDa) GFAP over calpain cleavage products (37-39kDa) with orthogonal fit for equal error weights, R^2 and FDR-corrected Logworth ($\log_{10}$p-values, false discovery rate corrected). **C)** Bivariate graph of GFAP BDP co-products show greater missingness among 15-19kDa versus 20-26kDa bandsets (circled, 28% or 15 more zeroes; orthogonal fit, FDR-corrected Logworth).

Figure 8: Dynamic GFAP proteolysis differentiates poor from good TBI patient outcome not full-length GFAP profiles
Shown are trajectories of GFAP molecular weights over 10PIDs partitioned by good recovery (GOSE 5-8) versus poor outcome (GOSE1-4) with mean cubic splines and 95% confidence bands (24 patients; 102 observations). **A)** Calpain generated 37-39kDa GFAP BDP trajectories differed in outcome by 1.1SD unit ($p=0.02$, adjusted for elapsed time and age effects; subject ID as random effect). **B)** Small GFAP-BDPs (20-26kDa) showed 0.9SD mean higher levels in patients with poor recovery over time than those with good recovery with trends influenced by age and missingness.
C) Full-length, 50kDa GFAP profiles overlapped over time lacking differentiation between good versus poor outcome.

References

1. Maas AIR, Menon DK, Manley GT*, et al*. Traumatic brain injury: progress and challenges in prevention, clinical care, and research. *The Lancet Neurology*. 2022/11/01/ 2022;21(11):1004-1060. doi:https://doi.org/10.1016/S1474-4422(22)00309-X
2. Karamian A, Lucke-Wold B, Seifi A. Prevalence of Traumatic Brain Injury in the General Adult Population of the USA: A Meta-Analysis. *Neuroepidemiology*. Aug 22 2024:1-10. doi:10.1159/000540676
3. Nelson LD, Temkin NR, Barber J*, et al*. Functional Recovery, Symptoms, and Quality of Life 1 to 5 Years After Traumatic Brain Injury: Findings From the TRACK-TBI Study. *JAMA Network Open*. 2023;6(3):e233660-e233660. doi:10.1001/jamanetworkopen.2023.3660
4. Nelson LD, Temkin NR, Dikmen S*, et al*. Recovery After Mild Traumatic Brain Injury in Patients Presenting to US Level I Trauma Centers: A Transforming Research and Clinical Knowledge in

Traumatic Brain Injury (TRACK-TBI) Study. *JAMA neurology*. Jun 3 2019;doi:10.1001/jamaneurol.2019.1313
5. Ng SY, Lee AYW. Traumatic Brain Injuries: Pathophysiology and Potential Therapeutic Targets. Review. *Frontiers in Cellular Neuroscience*. 2019-November-27 2019;Volume 13 - 2019doi:10.3389/fncel.2019.00528
6. Giza CC, Hovda DA. The new neurometabolic cascade of concussion. *Neurosurgery*. Oct 2014;75 Suppl 4:S24-33. doi:10.1227/NEU.0000000000000505
7. Hillered L, Vespa PM, Hovda DA. Translational neurochemical research in acute human brain injury: the current status and potential future for cerebral microdialysis. *Journal of neurotrauma*. Jan 2005;22(1):3-41. doi:10.1089/neu.2005.22.3
8. Stovell MG, Helmy A, Thelin EP, Jalloh I, Hutchinson PJ, Carpenter KLH. An overview of clinical cerebral microdialysis in acute brain injury. *Frontiers in neurology*. 2023;14:1085540. doi:10.3389/fneur.2023.1085540
9. Wilson L, Newcombe VFJ, Whitehouse DP*, et al*. Association of early blood-based biomarkers and six-month functional outcomes in conventional severity categories of traumatic brain injury: capturing the continuous spectrum of injury. *eBioMedicine*. 2024;107doi:10.1016/j.ebiom.2024.105298
10. Bazarian JJ, Biberthaler P, Welch RD*, et al*. Serum GFAP and UCH-L1 for prediction of absence of intracranial injuries on head CT (ALERT-TBI): a multicentre observational study. *The Lancet Neurology*. Sep 2018;17(9):782-789. doi:10.1016/S1474-4422(18)30231-X
11. Okonkwo DO, Puffer RC, Puccio AM*, et al*. Point-of-Care Platform Blood Biomarker Testing of Glial Fibrillary Acidic Protein versus S100 Calcium-Binding Protein B for Prediction of Traumatic Brain Injuries: A Transforming Research and Clinical Knowledge in Traumatic Brain Injury Study. *Journal of neurotrauma*. Dec 1 2020;37(23):2460-2467. doi:10.1089/neu.2020.7140
12. Diaz-Arrastia R. Performance of Diagnostic Biomarkers for Traumatic Brain Injury Within the First Hour-Expanding Their Clinical Utility. *JAMA Netw Open*. Sep 3 2024;7(9):e2431102. doi:10.1001/jamanetworkopen.2024.31102
13. Thelin EP, Zeiler FA, Ercole A*, et al*. Serial Sampling of Serum Protein Biomarkers for Monitoring Human Traumatic Brain Injury Dynamics: A Systematic Review. *Frontiers in neurology*. 2017;8:300. doi:10.3389/fneur.2017.00300
14. Bazarian JJ, Zetterberg H, Buki A*, et al*. Blood-Based Biomarkers for Improved Characterization of Traumatic Brain Injury: Recommendations from the 2024 National Institute for Neurological Disorders and Stroke Traumatic Brain Injury Classification and Nomenclature Initiative Blood-Based Biomarkers Working Group. *Journal of neurotrauma*. May 20 2025;doi:10.1089/neu.2024.0581
15. Manley GT, Dams-O'Connor K, Alosco ML*, et al*. A new characterisation of acute traumatic brain injury: the NIH-NINDS TBI Classification and Nomenclature Initiative. *The Lancet Neurology*. Jun 2025;24(6):512-523. doi:10.1016/S1474-4422(25)00154-1
16. Wilde EA, Wanner IB, Kenney K*, et al*. A Framework to Advance Biomarker Development in the Diagnosis, Outcome Prediction, and Treatment of Traumatic Brain Injury. *Journal of neurotrauma*. Apr 2022;39(7-8):436-457. doi:10.1089/neu.2021.0099
17. Metting Z, Wilczak N, Rodiger LA, Schaaf JM, van der Naalt J. GFAP and S100B in the acute phase of mild traumatic brain injury. *Neurology*. May 1 2012;78(18):1428-33. doi:10.1212/WNL.0b013e318253d5c7
18. Papa L, Lewis LM, Silvestri S*, et al*. Serum levels of ubiquitin C-terminal hydrolase distinguish mild traumatic brain injury from trauma controls and are elevated in mild and moderate traumatic brain injury patients with intracranial lesions and neurosurgical intervention. *The journal of trauma and acute care surgery*. May 2012;72(5):1335-44. doi:10.1097/TA.0b013e3182491e3d

19. Pelinka LE, Kroepfl A, Schmidhammer R*, et al*. Glial fibrillary acidic protein in serum after traumatic brain injury and multiple trauma. *The Journal of trauma*. Nov 2004;57(5):1006-12.
20. Lumpkins KM, Bochicchio GV, Keledjian K, Simard JM, McCunn M, Scalea T. Glial fibrillary acidic protein is highly correlated with brain injury. *The Journal of trauma*. Oct 2008;65(4):778-82; discussion 782-4.
21. Robertson CS, Martinez FS, McQuillan LE*, et al*. Serial Measurements of Serum Glial Fibrillary Acidic Protein in Moderate-Severe Traumatic Brain Injury: Potential Utility in Providing Insights into Secondary Insults and Long-Term Outcome. *Journal of neurotrauma*. Jan 2024;41(1-2):73-90. doi:10.1089/neu.2023.0111
22. Papa L, McKinley WI, Valadka AB*, et al*. Diagnostic Performance of GFAP, UCH-L1, and MAP-2 Within 30 and 60 Minutes of Traumatic Brain Injury. *JAMA Network Open*. 2024;7(9):e2431115-e2431115. doi:10.1001/jamanetworkopen.2024.31115
23. Halford J, Shen S, Itamura K*, et al*. New astroglial injury-defined biomarkers for neurotrauma assessment. *Journal of cerebral blood flow and metabolism : official journal of the International Society of Cerebral Blood Flow and Metabolism*. Oct 2017;37(10):3278-3299. doi:10.1177/0271678X17724681
24. Papa L, Brophy GM, Welch RD*, et al*. Time Course and Diagnostic Accuracy of Glial and Neuronal Blood Biomarkers GFAP and UCH-L1 in a Large Cohort of Trauma Patients With and Without Mild Traumatic Brain Injury. *JAMA neurology*. May 1 2016;73(5):551-60. doi:10.1001/jamaneurol.2016.0039
25. Chen W, Nishikimi A, Kamata T, Adachi Y. A reducing and denaturing step maximizes the immunoprecipitations of m-calpain and I-2(PP2A)/SET: an approach toward antibodies that do not work well in immunoprecipitation. *J Biochem Biophys Methods*. Jul 31 2006;68(1):65-8. doi:10.1016/j.jbbm.2006.02.012
26. Michielsen EC, Diris JH, Hackeng CM, Wodzig WK, Van Dieijen-Visser MP. Highly sensitive immunoprecipitation method for extracting and concentrating low-abundance proteins from human serum. *Clinical chemistry*. Jan 2005;51(1):222-4. doi:10.1373/clinchem.2004.036251
27. Bons JA, Michielsen EC, de Boer D*, et al*. A specific immunoprecipitation method for isolating isoforms of insulin-like growth factor binding protein-3 from serum. *Clin Chim Acta*. Jan 2008;387(1-2):59-65. doi:10.1016/j.cca.2007.09.002
28. Jin Z, Fu Z, Yang J, Troncosco J, Everett AD, Van Eyk JE. Identification and characterization of citrulline-modified brain proteins by combining HCD and CID fragmentation. *Proteomics*. Sep 2013;13(17):2682-91. doi:10.1002/pmic.201300064
29. Han K-K, Richard C, Biserte G. Current developments in chemical cleavage of proteins. *International Journal of Biochemistry*. 1983/01/01/ 1983;15(7):875-884. doi:https://doi.org/10.1016/0020-711X(83)90162-3
30. Vestling MM, Kelly MA, Fenselau C. Optimization by mass spectrometry of a tryptophan-specific protein cleavage reaction. *Rapid Commun Mass Spectrom*. Sep 1994;8(9):786-90. doi:10.1002/rcm.1290080925
31. Kouklis PD, Traub P, Georgatos SD. Involvement of the consensus sequence motif at coil 2b in the assembly and stability of vimentin filaments. *Journal of cell science*. May 1992;102 (Pt 1):31-41. doi:10.1242/jcs.102.1.31
32. Pruss RM. Efficient detection of intermediate filament proteins using a panspecific monoclonal antibody: anti-IFA. *Journal of neuroimmunology*. Jun 1985;8(4-6):293-9. doi:10.1016/s0165-5728(85)80068-0
33. Wanner IB. An in vitro trauma model to study rodent and human astrocyte reactivity. *Methods in molecular biology*. 2012;814:189-219. doi:10.1007/978-1-61779-452-0_14

34. Chen MH, Hagemann TL, Quinlan RA, Messing A, Perng MD. Caspase cleavage of GFAP produces an assembly-compromised proteolytic fragment that promotes filament aggregation. *ASN neuro*. 2013;5(5):e00125. doi:10.1042/AN20130032
35. Chen YS, Lim SC, Chen MH, Quinlan RA, Perng MD. Alexander disease causing mutations in the C-terminal domain of GFAP are deleterious both to assembly and network formation with the potential to both activate caspase 3 and decrease cell viability. *Exp Cell Res*. Oct 1 2011;317(16):2252-66. doi:10.1016/j.yexcr.2011.06.017
36. Ishigami A, Masutomi H, Handa S*, et al*. Mass spectrometric identification of citrullination sites and immunohistochemical detection of citrullinated glial fibrillary acidic protein in Alzheimer's disease brains. *Journal of neuroscience research*. Nov 2015;93(11):1664-74. doi:10.1002/jnr.23620
37. Lee MS, Kwon YT, Li M, Peng J, Friedlander RM, Tsai LH. Neurotoxicity induces cleavage of p35 to p25 by calpain. *Nature*. May 18 2000;405(6784):360-4. doi:10.1038/35012636
38. Yap YW, Whiteman M, Bay BH*, et al*. Hypochlorous acid induces apoptosis of cultured cortical neurons through activation of calpains and rupture of lysosomes. *Journal of neurochemistry*. Sep 2006;98(5):1597-609. doi:10.1111/j.1471-4159.2006.03996.x
39. Ekert PG, Silke J, Vaux DL. Caspase inhibitors. *Cell death and differentiation*. Nov 1999;6(11):1081-6. doi:10.1038/sj.cdd.4400594
40. Knoblach SM, Alroy DA, Nikolaeva M, Cernak I, Stoica BA, Faden AI. Caspase inhibitor z-DEVD-fmk attenuates calpain and necrotic cell death in vitro and after traumatic brain injury. *Journal of cerebral blood flow and metabolism : official journal of the International Society of Cerebral Blood Flow and Metabolism*. Oct 2004;24(10):1119-32. doi:10.1097/01.WCB.0000138664.17682.32
41. Kroes ADA, Finley JR. Demystifying omega squared: Practical guidance for effect size in common analysis of variance designs. *Psychol Methods*. Jul 20 2023;doi:10.1037/met0000581
42. Nelson PR, Wludyka PS, Copeland KAF. Analysis of Means: A Graphical Method for Comparing Means, Rates and Proportions. *Asa Siam Ser Stat Ap*. 2005;18:1-247. doi:10.1137/1.9780898718362
43. Hsu JC, Nelson B. Multiple comparisons in the general linear model. *J Comput Graph Stat*. Mar 1998;7(1):23-41. doi:Doi 10.2307/1390767
44. Lakens D. Calculating and reporting effect sizes to facilitate cumulative science: a practical primer for t-tests and ANOVAs. Review. *Frontiers in Psychology*. 2013-November-26 2013;4doi:10.3389/fpsyg.2013.00863
45. Lakshmi R, Sajesh TA. A robust distance-based approach for detecting multidimensional outliers. *J Appl Stat*. 2025;52(6):1278-1298. doi:10.1080/02664763.2024.2422403
46. Van Aelst S, Van Driessen K, Rousseeuw PJ. A robust method for multivariate regression. *St Class Dat Anal*. 2000:309-314.
47. Habshah M, Sani M, Arasan J. Robust Heteroscedasticity Consistent Covariance Matrix Estimator based on Robust Mahalanobis Distance and Diagnostic Robust Generalized Potential Weighting Methods in Linear Regression. *J Mod Appl Stat Meth*. May 2018;17(1)doi:ARTN 17

10.22237/jmasm/1530279855
48. Shi Y, Mowery RA, Ashley J*, et al*. Abnormal SDS-PAGE migration of cytosolic proteins can identify domains and mechanisms that control surfactant binding. *Protein Sci*. Aug 2012;21(8):1197-209. doi:10.1002/pro.2107
49. Guan Y, Zhu Q, Huang D, Zhao S, Jan Lo L, Peng J. An equation to estimate the difference between theoretically predicted and SDS PAGE-displayed molecular weights for an acidic peptide. *Scientific reports*. Aug 27 2015;5:13370. doi:10.1038/srep13370

50. Inagaki M, Nakamura Y, Takeda M, Nishimura T, Inagaki N. Glial fibrillary acidic protein: dynamic property and regulation by phosphorylation. *Brain pathology*. Jul 1994;4(3):239-43. doi:10.1111/j.1750-3639.1994.tb00839.x
51. Boyd SE, Nair B, Ng SW, Keith JM, Orian JM. Computational Characterization of 3' Splice Variants in the GFAP Isoform Family. *PloS one*. 2012;7(3):e33565. doi:10.1371/journal.pone.0033565
52. Mouser PE, Head E, Ha KH, Rohn TT. Caspase-mediated cleavage of glial fibrillary acidic protein within degenerating astrocytes of the Alzheimer's disease brain. *The American journal of pathology*. Mar 2006;168(3):936-46. doi:10.2353/ajpath.2006.050798
53. Yang Z, Arja RD, Zhu T*, et al*. Characterization of Calpain and Caspase-6-Generated Glial Fibrillary Acidic Protein Breakdown Products Following Traumatic Brain Injury and Astroglial Cell Injury. *International Journal of Molecular Sciences*. 2022;23(16):8960.
54. Kim B, Kim S, Jin MS. Crystal structure of the human glial fibrillary acidic protein 1B domain. *Biochemical and biophysical research communications*. Sep 18 2018;503(4):2899-2905. doi:10.1016/j.bbrc.2018.08.066
55. Deng Y, Thompson BM, Gao X, Hall ED. Temporal relationship of peroxynitrite-induced oxidative damage, calpain-mediated cytoskeletal degradation and neurodegeneration after traumatic brain injury. *Experimental neurology*. May 2007;205(1):154-65. doi:10.1016/j.expneurol.2007.01.023
56. Knoblach SM, Nikolaeva M, Huang X*, et al*. Multiple caspases are activated after traumatic brain injury: evidence for involvement in functional outcome. *Journal of neurotrauma*. Oct 2002;19(10):1155-70. doi:10.1089/08977150260337967
57. Baudry M, Luo YL, Bi X. Calpain-2 Inhibitors as Therapy for Traumatic Brain Injury. *Neurotherapeutics : the journal of the American Society for Experimental NeuroTherapeutics*. Oct 2023;20(6):1592-1602. doi:10.1007/s13311-023-01407-y
58. Dhani S, Zhao Y, Zhivotovsky B. A long way to go: caspase inhibitors in clinical use. *Cell Death & Disease*. 2021/10/15 2021;12(10):949. doi:10.1038/s41419-021-04240-3
59. Liu MC, Akle V, Zheng W*, et al*. Comparing calpain- and caspase-3-mediated degradation patterns in traumatic brain injury by differential proteome analysis. *The Biochemical journal*. Mar 15 2006;394(Pt 3):715-25.
60. Pike BR, Flint J, Dutta S, Johnson E, Wang KK, Hayes RL. Accumulation of non-erythroid alpha II-spectrin and calpain-cleaved alpha II-spectrin breakdown products in cerebrospinal fluid after traumatic brain injury in rats. *Journal of neurochemistry*. Sep 2001;78(6):1297-306.
61. Deng Y, Thompson BM, Gao X, Hall ED. Temporal Relationship of Peroxynitrite-Induced Oxidative Damage, Calpain-Mediated Cytoskeletal Degradation and Neurodegeneration after Traumatic Brain Injury. *Exp Neurol*. 2007;205(1):154.
62. McCracken E, Hunter AJ, Patel S, Graham DI, Dewar D. Calpain activation and cytoskeletal protein breakdown in the corpus callosum of head-injured patients. *Journal of neurotrauma*. Sep 1999;16(9):749-61.
63. Pineda JA, Lewis SB, Valadka AB*, et al*. Clinical significance of alphaII-spectrin breakdown products in cerebrospinal fluid after severe traumatic brain injury. *Journal of neurotrauma*. Feb 2007;24(2):354-66. doi:10.1089/neu.2006.003789
64. Stankewich MC, Cianci CD, Stabach PR, Ji L, Nath A, Morrow JS. Cell organization, growth, and neural and cardiac development require αII-spectrin. *Journal of cell science*. 2011;124(23):3956-3966. doi:10.1242/jcs.080374
65. Ringger NC, O'Steen BE, Brabham JG*, et al*. A novel marker for traumatic brain injury: CSF alphaII-spectrin breakdown product levels. *Journal of neurotrauma*. Oct 2004;21(10):1443-56.

66. Farkas O, Polgar B, Szekeres-Bartho J, Doczi T, Povlishock JT, Buki A. Spectrin breakdown products in the cerebrospinal fluid in severe head injury--preliminary observations. *Acta neurochirurgica*. Aug 2005;147(8):855-61.
67. Beer R, Franz G, Srinivasan A*, et al*. Temporal profile and cell subtype distribution of activated caspase-3 following experimental traumatic brain injury. *Journal of neurochemistry*. Sep 2000;75(3):1264-73.
68. Machnicka B, Ponceau A, Picot J, Colin Y, Lecomte MC. Deficiency of αII-spectrin affects endothelial cell-matrix contact and migration leading to impairment of angiogenesis in vitro. *Cell Mol Biol Lett*. 2020;25:3. doi:10.1186/s11658-020-0200-y
69. Machnicka B, Grochowalska R, Bogusławska DM, Sikorski AF, Lecomte MC. Spectrin-based skeleton as an actor in cell signaling. *Cell Mol Life Sci*. Jan 2012;69(2):191-201. doi:10.1007/s00018-011-0804-5
70. Kim JH, Kwon SJ, Stankewich MC, Huh GY, Glantz SB, Morrow JS. Reactive protoplasmic and fibrous astrocytes contain high levels of calpain-cleaved alpha 2 spectrin. *Exp Mol Pathol*. Feb 2016;100(1):1-7. doi:10.1016/j.yexmp.2015.11.005
71. Roberts-Lewis JM, Savage MJ, Marcy VR, Pinsker LR, Siman R. Immunolocalization of calpain I-mediated spectrin degradation to vulnerable neurons in the ischemic gerbil brain. *The Journal of neuroscience : the official journal of the Society for Neuroscience*. Jun 1994;14(6):3934-44.
72. Siman R, Shahim P, Tegner Y, Blennow K, Zetterberg H, Smith DH. Serum SNTF Increases in Concussed Professional Ice Hockey Players and Relates to the Severity of Postconcussion Symptoms. *Journal of neurotrauma*. Sep 1 2015;32(17):1294-300. doi:10.1089/neu.2014.3698
73. Phillips CL, Faridounnia M, Armao D, Snider NT. Stability dynamics of neurofilament and GFAP networks and protein fragments. *Current opinion in cell biology*. Dec 2023;85:102266. doi:10.1016/j.ceb.2023.102266
74. Zoltewicz JS, Scharf D, Yang B, Chawla A, Newsom KJ, Fang L. Characterization of Antibodies that Detect Human GFAP after Traumatic Brain Injury. *Biomark Insights*. 2012;7:71-9. doi:10.4137/BMI.S9873
75. Kampfl A, Posmantur R, Nixon R*, et al*. mu-calpain activation and calpain-mediated cytoskeletal proteolysis following traumatic brain injury. *Journal of neurochemistry*. Oct 1996;67(4):1575-83.
76. Schoch KM, von Reyn CR, Bian J, Telling GC, Meaney DF, Saatman KE. Brain Injury-Induced Proteolysis Is Reduced in a Novel Calpastatin Overexpressing Transgenic Mouse. *J Neurochem*. 2013;125(6):909.
77. Aleksandrova MA, Sukhinich KK. Astrocytes of the Brain: Retinue Plays the King. *Russ J Dev Biol+*. Aug 2022;53(4):252-271. doi:10.1134/S1062360422040026
78. Sedmak G, Jovanov-Milošević N, Puskarjov M*, et al*. Developmental Expression Patterns of KCC2 and Functionally Associated Molecules in the Human Brain. *Cerebral cortex*. 2016;26(12):4574-4589. doi:10.1093/cercor/bhv218
79. Colombo JA, Yanez A, Lipina SJ. Interlaminar astroglial processes in the cerebral cortex of non human primates: response to injury. *J Hirnforsch*. 1997;38(4):503-12.
80. Verkhratsky A, Butt A, Li B*, et al*. Astrocytes in human central nervous system diseases: a frontier for new therapies. *Signal Transduct Target Ther*. Oct 13 2023;8(1):396. doi:10.1038/s41392-023-01628-9
81. Caballero B, Bourdenx M, Luengo E*, et al*. Acetylated tau inhibits chaperone-mediated autophagy and promotes tau pathology propagation in mice. *Nature Communications*. 2021/04/14 2021;12(1):2238. doi:10.1038/s41467-021-22501-9

82. Kabir F, Atkinson R, Cook AL, Phipps AJ, King AE. The role of altered protein acetylation in neurodegenerative disease. Review. *Frontiers in Aging Neuroscience*. 2023-January-04 2023;14doi:10.3389/fnagi.2022.1025473
83. Lazarus RC, Buonora JE, Flora MN*, et al*. Protein Citrullination: A Proposed Mechanism for Pathology in Traumatic Brain Injury. Original Research. *Frontiers in neurology*. 2015-September-22 2015;6doi:10.3389/fneur.2015.00204
84. Wang B, Fields L, Li L. Recent advances in characterization of citrullination and its implication in human disease research: From method development to network integration. *Proteomics*. Nov 2023;23(21-22):e2200286. doi:10.1002/pmic.202200286
85. Lazarus RC, Buonora JE, Flora MN*, et al*. Protein Citrullination: A Proposed Mechanism for Pathology in Traumatic Brain Injury. *Frontiers in neurology*. 2015;6:204. doi:10.3389/fneur.2015.00204
86. Messing A, Brenner M. GFAP at 50. *ASN neuro*. Jan-Dec 2020;12:1759091420949680. doi:10.1177/1759091420949680
87. Ishigami A, Ohsawa T, Hiratsuka M*, et al*. Abnormal accumulation of citrullinated proteins catalyzed by peptidylarginine deiminase in hippocampal extracts from patients with Alzheimer's disease. *Journal of neuroscience research*. Apr 1 2005;80(1):120-8. doi:10.1002/jnr.20431
88. Wizeman JW, Nicholas AP, Ishigami A, Mohan R. Citrullination of glial intermediate filaments is an early response in retinal injury. *Mol Vis*. 2016;22:1137-1155.
89. Nicholas AP, Sambandam T, Echols JD, Barnum SR. Expression of citrullinated proteins in murine experimental autoimmune encephalomyelitis. *The Journal of comparative neurology*. Jun 6 2005;486(3):254-66. doi:10.1002/cne.20527
90. Lee YB, Du S, Rhim H, Lee EB, Markelonis GJ, Oh TH. Rapid increase in immunoreactivity to GFAP in astrocytes in vitro induced by acidic pH is mediated by calcium influx and calpain I. *Brain research*. May 12 2000;864(2):220-9.
91. Popov A, Brazhe A, Denisov P*, et al*. Astrocyte dystrophy in ageing brain parallels impaired synaptic plasticity. *Aging Cell*. Mar 2021;20(3):e13334. doi:10.1111/acel.13334
92. Vagberg M, Norgren N, Dring A*, et al*. Levels and Age Dependency of Neurofilament Light and Glial Fibrillary Acidic Protein in Healthy Individuals and Their Relation to the Brain Parenchymal Fraction. *PloS one*. 2015;10(8):e0135886. doi:10.1371/journal.pone.0135886
93. Cooper JG, Stukas S, Ghodsi M*, et al*. Age specific reference intervals for plasma biomarkers of neurodegeneration and neurotrauma in a Canadian population. *Clinical biochemistry*. Nov 2023;121-122:110680. doi:10.1016/j.clinbiochem.2023.110680
94. Li LM, Kodosaki E, Heslegrave A*, et al*. High-dimensional proteomic analysis for pathophysiological classification of traumatic brain injury. *Brain : a journal of neurology*. 2024;148(3):1015-1030. doi:10.1093/brain/awae305
95. Inekci D, Jonesco DS, Kennard S, Karsdal MA, Henriksen K. The potential of pathological protein fragmentation in blood-based biomarker development for dementia - with emphasis on Alzheimer's disease. *Frontiers in neurology*. 2015;6:90. doi:10.3389/fneur.2015.00090
96. Nielsen P, Olsen MH, Willer-Hansen RS*, et al*. Ventriculostomy-associated infection (VAI) in patients with acute brain injury-a retrospective study. *Acta neurochirurgica*. Mar 11 2024;166(1):128. doi:10.1007/s00701-024-06018-w
97. Jha RM, Kochanek PM, Simard JM. Pathophysiology and treatment of cerebral edema in traumatic brain injury. *Neuropharmacology*. Feb 2019;145(Pt B):230-246. doi:10.1016/j.neuropharm.2018.08.004
98. Korley F, Pauls Q, Yeatts SD*, et al*. Progesterone Treatment Does Not Decrease Serum Levels of Biomarkers of Glial and Neuronal Cell Injury in Moderate and Severe Traumatic Brain Injury

Subjects: A Secondary Analysis of the Progesterone for Traumatic Brain Injury, Experimental Clinical Treatment (ProTECT) III Trial. *J Neurotrauma*. 2021;38(14):1953.
99. Shreiber DI, Bain AC, Ross DT*, et al*. Experimental investigation of cerebral contusion: histopathological and immunohistochemical evaluation of dynamic cortical deformation. *Journal of neuropathology and experimental neurology*. Feb 1999;58(2):153-64.
100. Farkas O, Povlishock JT. Cellular and subcellular change evoked by diffuse traumatic brain injury: a complex web of change extending far beyond focal damage. *Prog Brain Res*. 2007;161:43-59.
101. Farkas O, Lifshitz J, Povlishock JT. Mechanoporation induced by diffuse traumatic brain injury: an irreversible or reversible response to injury? *The Journal of neuroscience : the official journal of the Society for Neuroscience*. Mar 22 2006;26(12):3130-40.
102. Levine J, Kwon E, Paez P*, et al*. Traumatically injured astrocytes release a proteomic signature modulated by STAT3-dependent cell survival. *Glia*. Dec 19 2015;doi:10.1002/glia.22953
103. Barbee KA. Mechanical cell injury. *Ann N Y Acad Sci*. Dec 2005;1066:67-84. doi:10.1196/annals.1363.006
104. Dobson J, Kumar A, Willis LF*, et al*. Inducing protein aggregation by extensional flow. *Proceedings of the National Academy of Sciences*. 2017;114(18):4673-4678. doi:doi:10.1073/pnas.1702724114
105. Rolleke U, Kumari P, Meyer R, Koster S. The unique biomechanics of intermediate filaments - From single filaments to cells and tissues. *Current opinion in cell biology*. Dec 2023;85:102263. doi:10.1016/j.ceb.2023.102263
106. Karl J, Gottfried C, Tramontina F, Dunkley P, Rodnight R, Goncalves CA. GFAP phosphorylation studied in digitonin-permeabilized astrocytes: standardization of conditions. *Brain research*. Jan 17 2000;853(1):32-40.
107. Block J, Witt H, Candelli A*, et al*. Nonlinear Loading-Rate-Dependent Force Response of Individual Vimentin Intermediate Filaments to Applied Strain. *Phys Rev Lett*. Jan 27 2017;118(4):048101. doi:10.1103/PhysRevLett.118.048101
108. Ammendolia DA, Bement WM, Brumell JH. Plasma membrane integrity: implications for health and disease. *BMC Biol*. Apr 13 2021;19(1):71. doi:10.1186/s12915-021-00972-y
109. Guo J, Yang WT, Mai FY*, et al*. Unravelling oncosis: morphological and molecular insights into a unique cell death pathway. *Front Immunol*. 2024;15:1450998. doi:10.3389/fimmu.2024.1450998
110. Majno G, Joris I. Apoptosis, oncosis, and necrosis. An overview of cell death. *The American journal of pathology*. Jan 1995;146(1):3-15.
111. Chu X, Fu X, Zou L*, et al*. Oncosis, the possible cell death pathway in astrocytes after focal cerebral ischemia. *Brain research*. May 29 2007;1149:157-64. doi:10.1016/j.brainres.2007.02.061
112. Loh KY, Wang Z, Liao P. Oncotic Cell Death in Stroke. *Rev Physiol Biochem Pharmacol*. 2019;176:37-64. doi:10.1007/112_2018_13
113. Bondarenko A, Chesler M. Calcium dependence of rapid astrocyte death induced by transient hypoxia, acidosis, and extracellular ion shifts. *Glia*. Apr 15 2001;34(2):143-9.
114. Vlodavsky E, Palzur E, Shehadeh M, Soustiel JF. Post-traumatic cytotoxic edema is directly related to mitochondrial function. *Journal of cerebral blood flow and metabolism : official journal of the International Society of Cerebral Blood Flow and Metabolism*. Jan 2017;37(1):166-177. doi:10.1177/0271678X15621068
115. Bullock R, Maxwell WL, Graham DI, Teasdale GM, Adams JH. Glial swelling following human cerebral contusion: an ultrastructural study. *Journal of neurology, neurosurgery, and psychiatry*. May 1991;54(5):427-34.
116. Vespa P, Bergsneider M, Hattori N*, et al*. Metabolic crisis without brain ischemia is common after traumatic brain injury: a combined microdialysis and positron emission tomography study.

Journal of cerebral blood flow and metabolism : official journal of the International Society of Cerebral Blood Flow and Metabolism. Jun 2005;25(6):763-74. doi:10.1038/sj.jcbfm.9600073
117. Zhu X, Tao L, Tejima-Mandeville E*, et al*. Plasmalemma permeability and necrotic cell death phenotypes after intracerebral hemorrhage in mice. *Stroke; a journal of cerebral circulation*. Feb 2012;43(2):524-31. doi:10.1161/STROKEAHA.111.635672
118. Whalen MJ, Dalkara T, You Z*, et al*. Acute plasmalemma permeability and protracted clearance of injured cells after controlled cortical impact in mice. *Journal of cerebral blood flow and metabolism : official journal of the International Society of Cerebral Blood Flow and Metabolism*. Mar 2008;28(3):490-505. doi:10.1038/sj.jcbfm.9600544
119. Li DR, Zhang F, Wang Y*, et al*. Quantitative analysis of GFAP- and S100 protein-immunopositive astrocytes to investigate the severity of traumatic brain injury. *Leg Med (Tokyo)*. Mar 2012;14(2):84-92. doi:10.1016/j.legalmed.2011.12.007
120. DeArmond SJ, Fajardo M, Naughton SA, Eng LF. Degradation of glial fibrillary acidic protein by a calcium dependent proteinase: an electroblot study. *Brain research*. Mar 7 1983;262(2):275-82.
121. Ciesielski-Treska J, Goetschy JF, Aunis D. Proteolytic degradation of vimentin and glial fibrillary acidic protein in rat astrocytes in primary culture. *European journal of biochemistry / FEBS*. Feb 1 1984;138(3):465-71.
122. Phillips CL, Fu D, Herring LE, Armao D, Snider NT. Calpain-mediated proteolysis of vimentin filaments is augmented in giant axonal neuropathy fibroblasts exposed to hypotonic stress. *Front Cell Dev Biol*. 2022;10:1008542. doi:10.3389/fcell.2022.1008542
123. Byun Y, Chen F, Chang R, Trivedi M, Green KJ, Cryns VL. Caspase cleavage of vimentin disrupts intermediate filaments and promotes apoptosis. *Cell death and differentiation*. May 2001;8(5):443-50. doi:10.1038/sj.cdd.4400840
124. Metwally E, Al-Abbadi HA, Hussain T, Murtaza G, Abdellatif AM, Ahmed MF. Calpain signaling: from biology to therapeutic opportunities in neurodegenerative disorders. *Front Vet Sci*. 2023;10:1235163. doi:10.3389/fvets.2023.1235163
125. Liu G-Y, Xie W-L, Wang Y-T*, et al*. Calpain: the regulatory point of myocardial ischemia-reperfusion injury. Review. *Frontiers in Cardiovascular Medicine*. 2023-June-29 2023;Volume 10 - 2023doi:10.3389/fcvm.2023.1194402
126. Dias C, Nylandsted J. Plasma membrane integrity in health and disease: significance and therapeutic potential. *Cell Discovery*. 2021/01/19 2021;7(1):4. doi:10.1038/s41421-020-00233-2
127. Kilinc D, Gallo G, Barbee KA. Mechanical membrane injury induces axonal beading through localized activation of calpain. *Experimental neurology*. Oct 2009;219(2):553-61. doi:10.1016/j.expneurol.2009.07.014
128. Weber JT. Altered calcium signaling following traumatic brain injury. *Frontiers in pharmacology*. 2012;3:60. doi:10.3389/fphar.2012.00060
129. Gafni J, Cong X, Chen SF, Gibson BW, Ellerby LM. Calpain-1 cleaves and activates caspase-7. *The Journal of biological chemistry*. Sep 11 2009;284(37):25441-9. doi:10.1074/jbc.M109.038174
130. GOLL DE, THOMPSON VF, LI H, WEI W, CONG J. The Calpain System. *Physiological Reviews*. 2003;83(3):731-801. doi:10.1152/physrev.00029.2002
131. Pohl C, Dikic I. Cellular quality control by the ubiquitin-proteasome system and autophagy. *Science*. 2019;366(6467):818-822. doi:doi:10.1126/science.aax3769
132. Shields DC, Tyor WR, Deibler GE, Hogan EL, Banik NL. Increased calpain expression in activated glial and inflammatory cells in experimental allergic encephalomyelitis. *Proceedings of the National Academy of Sciences*. 1998;95(10):5768-5772. doi:doi:10.1073/pnas.95.10.5768
133. Acarin L, Villapol S, Faiz M, Rohn TT, Castellano B, Gonzalez B. Caspase-3 activation in astrocytes following postnatal excitotoxic damage correlates with cytoskeletal remodeling but not with cell death or proliferation. *Glia*. Jul 2007;55(9):954-65.

134. Conti AC, Raghupathi R, Trojanowski JQ, McIntosh TK. Experimental Brain Injury Induces Regionally Distinct Apoptosis during the Acute and Delayed Post-Traumatic Period. *J Neurosci*. 1998;18(15):5663.
135. Lafrenaye AD, McGinn MJ, Povlishock JT. Increased intracranial pressure after diffuse traumatic brain injury exacerbates neuronal somatic membrane poration but not axonal injury: evidence for primary intracranial pressure-induced neuronal perturbation. *Journal of cerebral blood flow and metabolism : official journal of the International Society of Cerebral Blood Flow and Metabolism*. Oct 2012;32(10):1919-32. doi:10.1038/jcbfm.2012.95
136. Lin NH, Yang AW, Chang CH, Perng MD. Elevated GFAP isoform expression promotes protein aggregation and compromises astrocyte function. *FASEB journal : official publication of the Federation of American Societies for Experimental Biology*. May 2021;35(5):e21614. doi:10.1096/fj.202100087R
137. Battaglia RA, Beltran AS, Delic S*, et al*. Site-specific phosphorylation and caspase cleavage of GFAP are new markers of Alexander disease severity. *Elife*. Nov 4 2019;8doi:10.7554/eLife.47789
138. Sambandam T, Belousova M, Accaviti-Loper MA*, et al*. Increased peptidylarginine deiminase type II in hypoxic astrocytes. *Biochemical and biophysical research communications*. Dec 24 2004;325(4):1324-9. doi:10.1016/j.bbrc.2004.10.173
139. Algeciras ME, Takahara H, Bhattacharya SK. Mechanical stretching elevates peptidyl arginine deiminase 2 expression in astrocytes. *Curr Eye Res*. Nov 2008;33(11):994-1001. doi:10.1080/02713680802447113
140. Jones JR, Kong L, Hanna MGt*, et al*. Mutations in GFAP Disrupt the Distribution and Function of Organelles in Human Astrocytes. *Cell Rep*. Oct 23 2018;25(4):947-958.e4. doi:10.1016/j.celrep.2018.09.083
141. Sosunov A, Olabarria M, Goldman JE. Alexander disease: an astrocytopathy that produces a leukodystrophy. *Brain pathology*. May 2018;28(3):388-398. doi:10.1111/bpa.12601
142. Xiong L, Sun L, Liu S, Zhu X, Teng Z, Yan J. The Protective Roles of Urinary Trypsin Inhibitor in Brain Injury Following Fat Embolism Syndrome in a Rat Model. *Cell Transplant*. Jun 2019;28(6):704-712. doi:10.1177/0963689718814766
143. Fereidoni M, Sabouni F, Moghimi A, Hosseini S. The effects of trypsin on rat brain astrocyte activation. *Iran J Neurol*. 2013;12(4):129-35.
144. Gae DD, Budamagunta MS, Hess JF*, et al*. Completion of the Vimentin Rod Domain Structure Using Experimental Restraints: A New Tool for Exploring Intermediate Filament Assembly and Mutations. *Structure*. Oct 1 2019;27(10):1547-1560.e4. doi:10.1016/j.str.2019.07.011
145. Strelkov SV, Herrmann H, Geisler N*, et al*. Conserved segments 1A and 2B of the intermediate filament dimer: their atomic structures and role in filament assembly. *The EMBO journal*. 2002;21(6):1255-1266. doi:https://doi.org/10.1093/emboj/21.6.1255
146. Jany PL, Agosta GE, Benko WS*, et al*. CSF and Blood Levels of GFAP in Alexander Disease. *eneuro*. 2015;2(5):ENEURO.0080-15.2015. doi:10.1523/eneuro.0080-15.2015
147. Iliff JJ, Lee H, Yu M*, et al*. Brain-wide pathway for waste clearance captured by contrast-enhanced MRI. *The Journal of clinical investigation*. Mar 2013;123(3):1299-309. doi:10.1172/JCI67677
148. Benedet AL, Milà-Alomà M, Vrillon A*, et al*. Differences Between Plasma and Cerebrospinal Fluid Glial Fibrillary Acidic Protein Levels Across the Alzheimer Disease Continuum. *JAMA neurology*. Dec 1 2021;78(12):1471-1483. doi:10.1001/jamaneurol.2021.3671
149. Hagemann TL, Boelens WC, Wawrousek EF, Messing A. Suppression of GFAP toxicity by alphaB-crystallin in mouse models of Alexander disease. *Human molecular genetics*. Apr 1 2009;18(7):1190-9. doi:10.1093/hmg/ddp013

150. Der Perng M, Su M, Wen SF*, et al*. The Alexander disease-causing glial fibrillary acidic protein mutant, R416W, accumulates into Rosenthal fibers by a pathway that involves filament aggregation and the association of alpha B-crystallin and HSP27. *Am J Hum Genet*. Aug 2006;79(2):197-213. doi:10.1086/504411
151. Rai M, Curley M, Coleman Z*, et al*. Analysis of proteostasis during aging with western blot of detergent-soluble and insoluble protein fractions. *STAR Protoc*. Sep 17 2021;2(3):100628. doi:10.1016/j.xpro.2021.100628
152. Sofroniew MV, Vinters HV. Astrocytes: biology and pathology. *Acta Neuropathol*. Jan 2010;119(1):7-35.
153. Escartin C, Galea E, Lakatos A*, et al*. Reactive astrocyte nomenclature, definitions, and future directions. *Nat Neurosci*. Mar 2021;24(3):312-325. doi:10.1038/s41593-020-00783-4
154. Pereira JB, Janelidze S, Smith R*, et al*. Plasma GFAP is an early marker of amyloid-β but not tau pathology in Alzheimer's disease. *Brain : a journal of neurology*. Dec 16 2021;144(11):3505-3516. doi:10.1093/brain/awab223
155. Saatman KE, Creed J, Raghupathi R. Calpain as a Therapeutic Target in Traumatic Brain Injury. *Neurotherapeutics : the journal of the American Society for Experimental NeuroTherapeutics*. 2010;7(1):31.
156. Madias MI, Stessman LN, Warlof SJ, Kudryashev JA, Kwon EJ. Spatial Measurement and Inhibition of Calpain Activity in Traumatic Brain Injury with an Activity-Based Nanotheranostic Platform. *ACS Nano*. 2024/09/17 2024;18(37):25565-25576. doi:10.1021/acsnano.4c06052
157. Zhang A, Zhang Z, Liu Y*, et al*. The Role of Caspase Family in Acute Brain Injury: The Potential Therapeutic Targets in the Future. *Current neuropharmacology*. 2022;20(6):1194-1211. doi:10.2174/1570159x19666211111121146
158. Knoblach SM, Huang X, VanGelderen J, Calva-Cerqueira D, Faden AI. Selective caspase activation may contribute to neurological dysfunction after experimental spinal cord trauma. *Journal of neuroscience research*. May 1 2005;80(3):369-80. doi:10.1002/jnr.20465
159. Faden AI, Movsesyan VA, Knoblach SM, Ahmed F, Cernak I. Neuroprotective effects of novel small peptides in vitro and after brain injury. *Neuropharmacology*. Sep 2005;49(3):410-24.
160. Adamczak SE, de Rivero Vaccari JP, Dale G*, et al*. Pyroptotic neuronal cell death mediated by the AIM2 inflammasome. *Journal of cerebral blood flow and metabolism : official journal of the International Society of Cerebral Blood Flow and Metabolism*. Apr 2014;34(4):621-9. doi:10.1038/jcbfm.2013.236
161. Harter L, Keel M, Hentze H, Leist M, Ertel W. Caspase-3 activity is present in cerebrospinal fluid from patients with traumatic brain injury. *Journal of neuroimmunology*. Dec 3 2001;121(1-2):76-8.
162. Diaz-Arrastia R, Kochanek PM, Bergold P*, et al*. Pharmacotherapy of traumatic brain injury: state of the science and the road forward: report of the Department of Defense Neurotrauma Pharmacology Workgroup. *Journal of neurotrauma*. Jan 15 2014;31(2):135-58. doi:10.1089/neu.2013.3019
163. Papa L, Lewis LM, Falk JL*, et al*. Elevated levels of serum glial fibrillary acidic protein breakdown products in mild and moderate traumatic brain injury are associated with intracranial lesions and neurosurgical intervention. *Annals of emergency medicine*. Jun 2012;59(6):471-83. doi:10.1016/j.annemergmed.2011.08.021
164. Zoltewicz JS, Mondello S, Yang B*, et al*. Biomarkers track damage after graded injury severity in a rat model of penetrating brain injury. *Journal of neurotrauma*. Jul 1 2013;30(13):1161-9. doi:10.1089/neu.2012.2762
165. Seidenfaden S-C, Kjerulff JL, Juul N*, et al*. Temporal Changes in Serum S100B Levels From Prehospital to Early In-Hospital Sampling in Patients Suffering Traumatic Brain Injury. Original

Research. *Frontiers in neurology*. 2022-April-08 2022;Volume 13 - 2022doi:10.3389/fneur.2022.800015
166. Lisi I, Moro F, Mazzone E*, et al*. Exploiting blood-based biomarkers to align preclinical models with human traumatic brain injury. *Brain : a journal of neurology*. Nov 9 2024;doi:10.1093/brain/awae350
167. Zhou Z, Zhao T, Gardus J*, et al*. Quantifying Ventricular CSF Clearance in the Human Brain Using Dynamic 18F-FDG PET: Insights into Age-Related Glymphatic Impairment. *medRxiv*. 2025:2025.04.07.25325241. doi:10.1101/2025.04.07.25325241
168. Gardner RC, Dams-O'Connor K, Morrissey MR, Manley GT. Geriatric Traumatic Brain Injury: Epidemiology, Outcomes, Knowledge Gaps, and Future Directions. *Journal of neurotrauma*. 2018/04/01 2017;35(7):889-906. doi:10.1089/neu.2017.5371
169. Chen CP, Chen RL, Preston JE. The influence of cerebrospinal fluid turnover on age-related changes in cerebrospinal fluid protein concentrations. *Neuroscience letters*. Jun 7 2010;476(3):138-41. doi:10.1016/j.neulet.2010.04.015
170. Kim JH, Im JG, Park SH. Measurement of changes in cerebrospinal fluid pulsation after traumatic brain injury using echo-planar imaging-based functional MRI. *NMR in biomedicine*. Mar 2024;37(3):e5061. doi:10.1002/nbm.5061
171. Bolte AC, Dutta AB, Hurt ME*, et al*. Meningeal lymphatic dysfunction exacerbates traumatic brain injury pathogenesis. *Nature Communications*. 2020/09/10 2020;11(1):4524. doi:10.1038/s41467-020-18113-4
172. Xiong G, Elkind JA, Kundu S*, et al*. Traumatic brain injury-induced ependymal ciliary loss decreases cerebral spinal fluid flow. *Journal of neurotrauma*. Aug 15 2014;31(16):1396-404. doi:10.1089/neu.2013.3110
173. Yeh P-H, Lippa SM, Brickell TA, Ollinger J, French LM, Lange RT. Longitudinal changes of white matter microstructure following traumatic brain injury in U.S. military service members. *Brain Communications*. 2022;4(3)doi:10.1093/braincomms/fcac132
174. Batista L, Stence NV, Mirsky DM*, et al*. Cytotoxic edema is associated with injury severity but not abusive mechanism in young children with traumatic brain injury. *Child Abuse & Neglect*. 2025/03/01/ 2025;161:107312. doi:https://doi.org/10.1016/j.chiabu.2025.107312
175. Newcombe VF, Williams GB, Outtrim JG*, et al*. Microstructural Basis of Contusion Expansion in Traumatic Brain Injury: Insights from Diffusion Tensor Imaging. *Journal of Cerebral Blood Flow & Metabolism*. 2013;33(6):855-862. doi:10.1038/jcbfm.2013.11
176. Zhang Y, Song S, Li Z, Huang B, Geng Y, Zhang L. The Application of Software "Rapid Processing of Perfusion and Diffusion" in Acute Ischemic Stroke. *Brain Sci*. Oct 27 2022;12(11)doi:10.3390/brainsci12111451
177. Turtzo LC, Luby M, Jikaria N*, et al*. Cytotoxic Edema Associated with Hemorrhage Predicts Poor Outcome after Traumatic Brain Injury. *Journal of neurotrauma*. Nov 15 2021;38(22):3107-3118. doi:10.1089/neu.2021.0037
178. Korley FK, Jain S, Sun X*, et al*. Prognostic value of day-of-injury plasma GFAP and UCH-L1 concentrations for predicting functional recovery after traumatic brain injury in patients from the US TRACK-TBI cohort: an observational cohort study. *The Lancet Neurology*. Sep 2022;21(9):803-813. doi:10.1016/S1474-4422(22)00256-3
179. Nylén K, Ost M, Csajbok LZ*, et al*. Increased serum-GFAP in patients with severe traumatic brain injury is related to outcome. *Journal of the neurological sciences*. Jan 15 2006;240(1-2):85-91. doi:10.1016/j.jns.2005.09.007
180. Pelinka LE, Kroepfl A, Leixnering M, Buchinger W, Raabe A, Redl H. GFAP versus S100B in serum after traumatic brain injury: relationship to brain damage and outcome. *Journal of neurotrauma*. Nov 2004;21(11):1553-61.

181. Kulbe JR, Jain S, Nelson LD*, et al*. Association of day-of-injury plasma glial fibrillary acidic protein concentration and six-month posttraumatic stress disorder in patients with mild traumatic brain injury. *Neuropsychopharmacology*. 2022/12/01 2022;47(13):2300-2308. doi:10.1038/s41386-022-01359-5
182. Wilson JE, Shinall MC, Jr., Leath TC*, et al*. Worse Than Death: Survey of Public Perceptions of Disability Outcomes After Hypothetical Traumatic Brain Injury. *Ann Surg*. Mar 1 2021;273(3):500-506. doi:10.1097/SLA.0000000000003389
183. Bhattacharyay S, Caruso PF, Åkerlund C*, et al*. Mining the contribution of intensive care clinical course to outcome after traumatic brain injury. *npj Digital Medicine*. 2023/08/21 2023;6(1):154. doi:10.1038/s41746-023-00895-8

Thumbnail

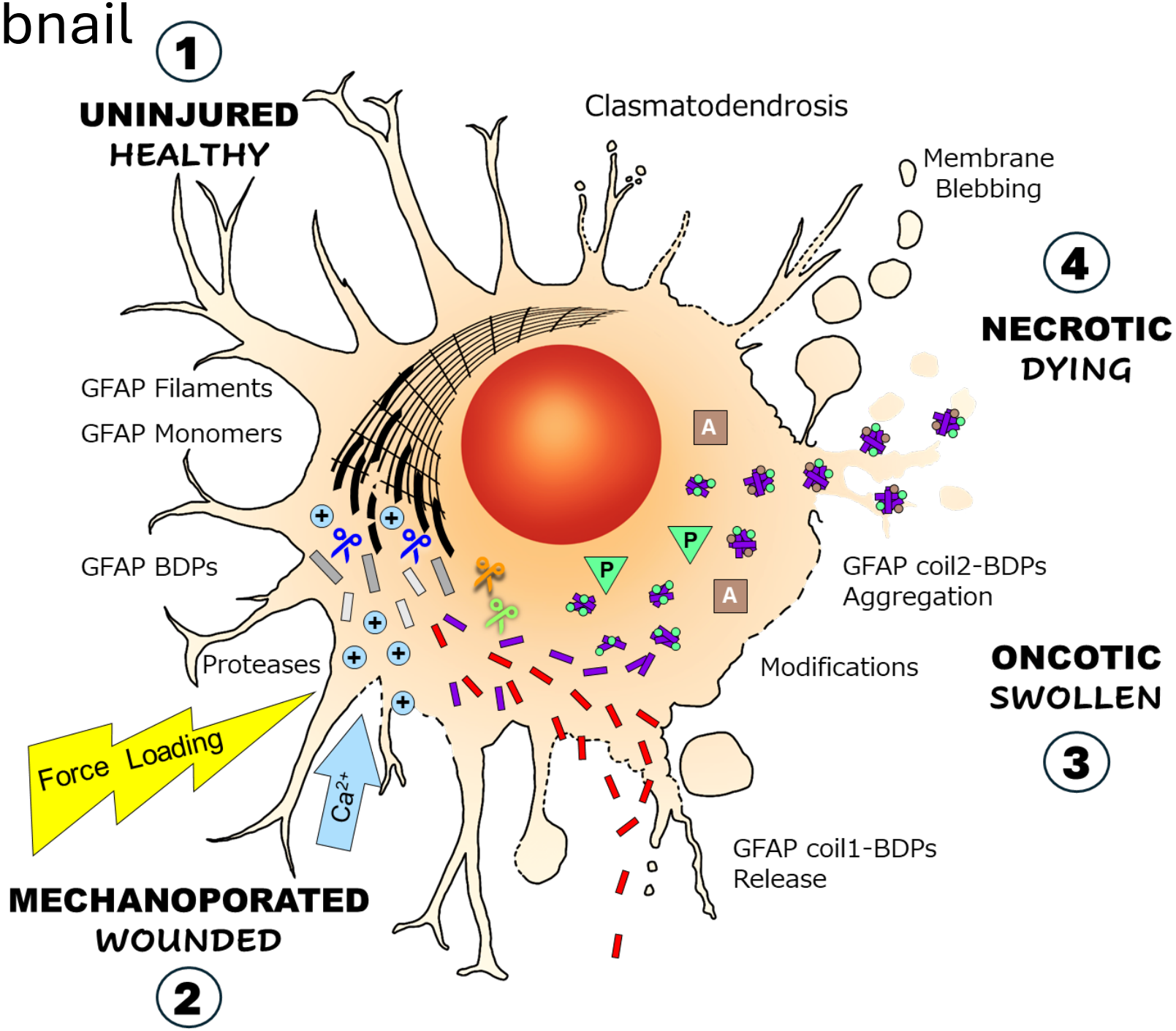

Symbol key

- GFAP Filaments
- GFAP Monomers +/- break
- Large GFAP-BDPs (42-49kDa)
- Calpain GFAP-BDPs (37-39kDa)
- Small GFAP Coil1-BDPs
- Small GFAP Coil2-BDPs
- GFAP Aggregates
- Calcium
- Peptidyl deiminases, PADs
- Citrullination
- Acetyltransferases
- Acetylation
- Calpain
- Caspase
- Endogenous Trypsin activity

Figure 1

A

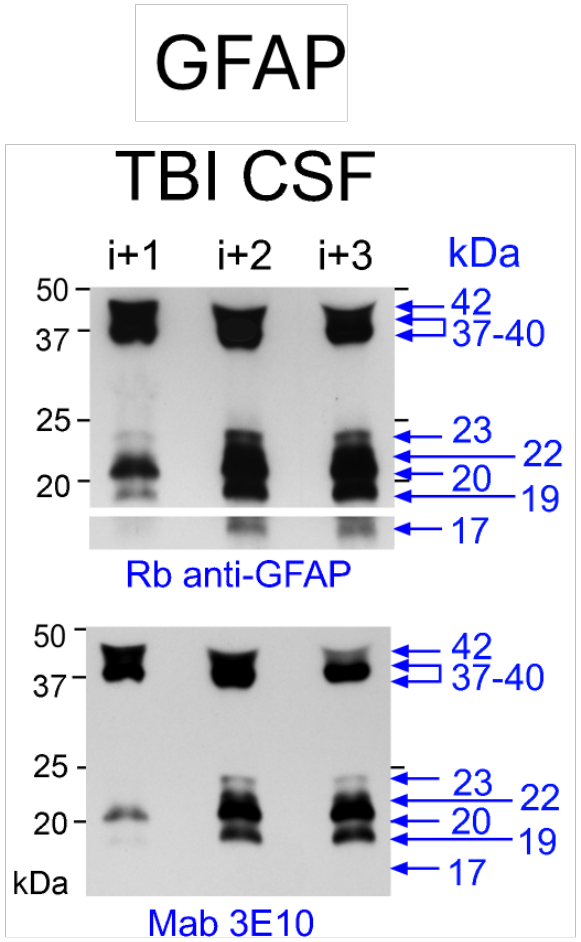

15% gel, 56ul CSF

B

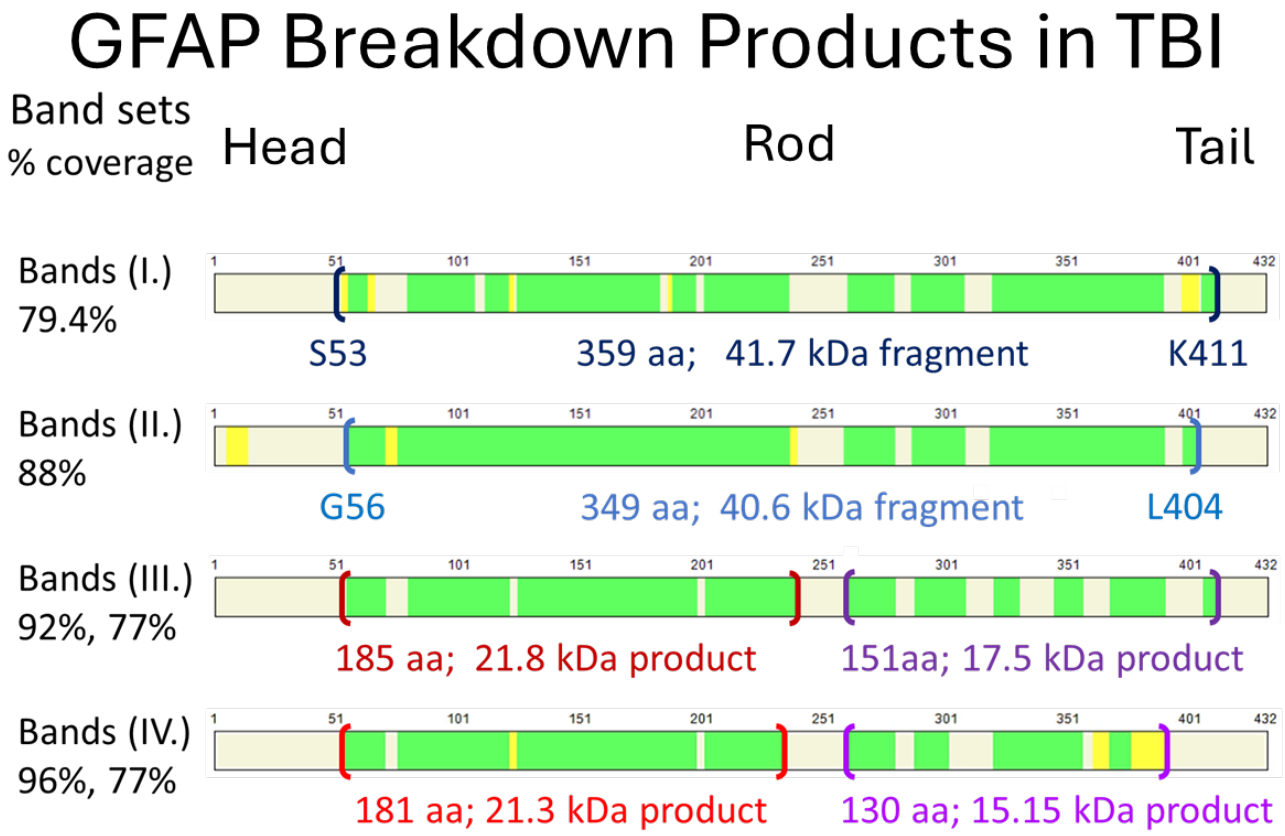

C

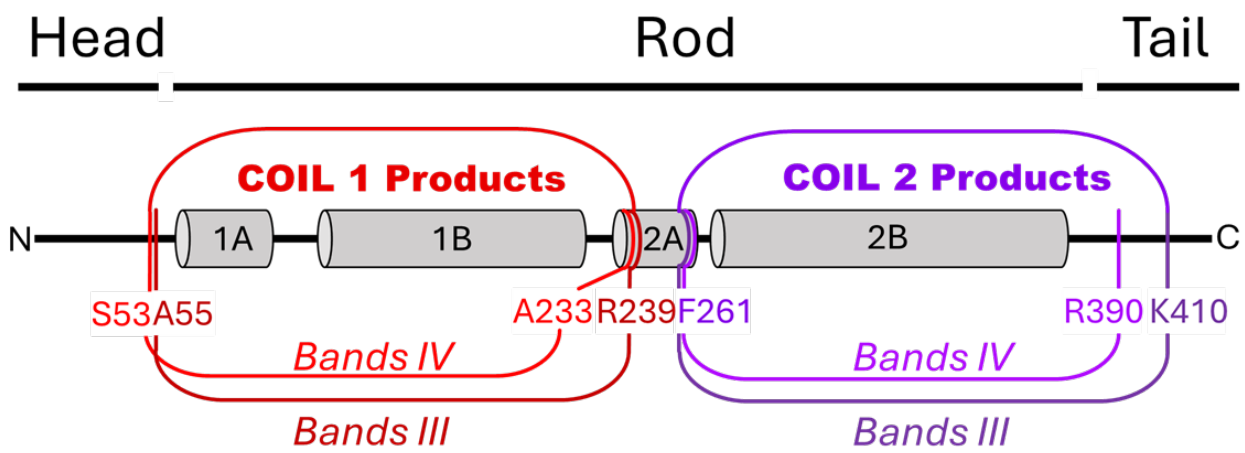

Figure 2

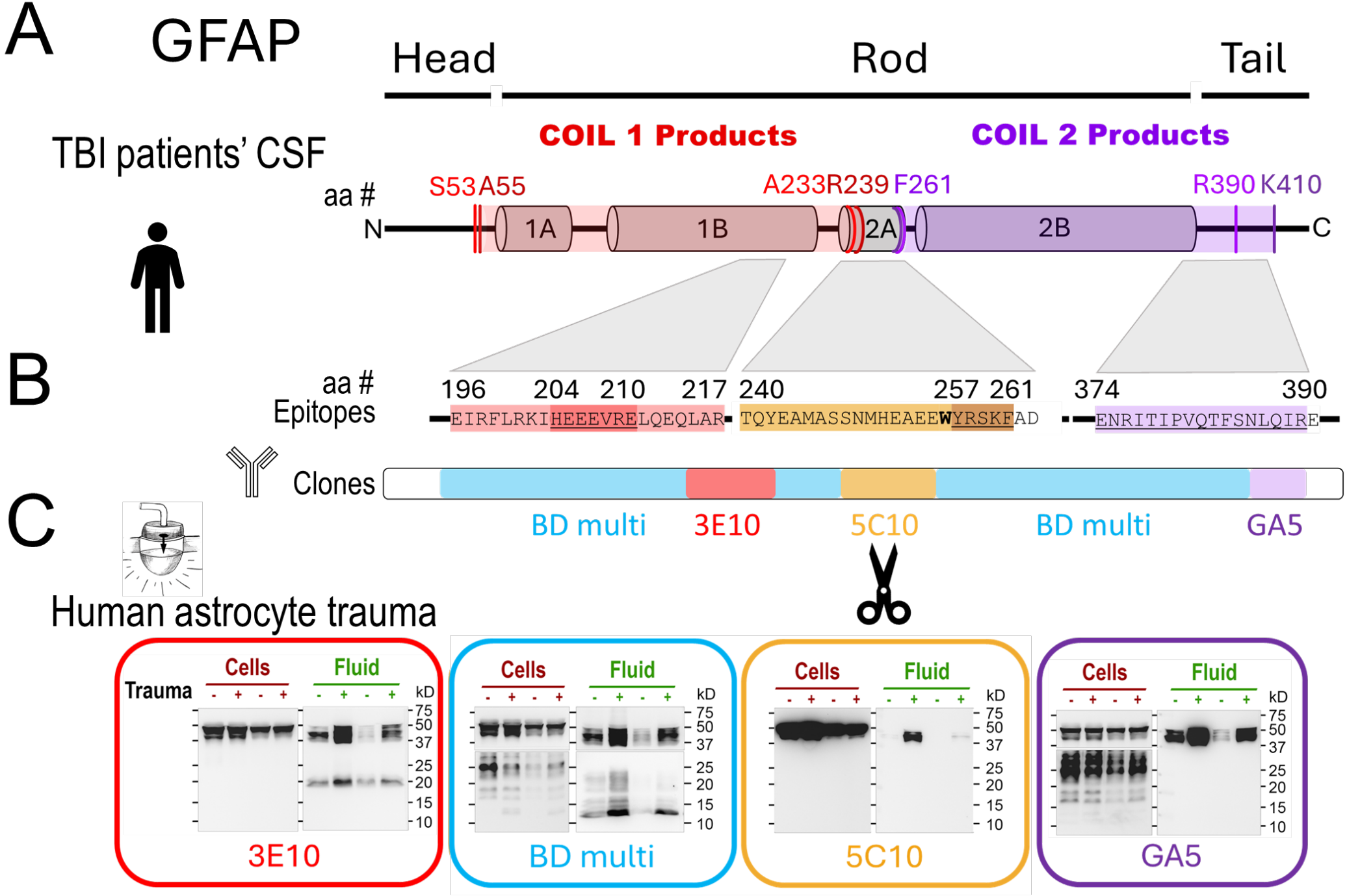
A
GFAP
Head
Rod
Tail
TBI patients' CSF
COIL 1 Products
COIL 2 Products
aa #
S53 A55
A233 R239 F261
R390 K410
N
1A
1B
2A
2B
C
B
aa #
196 204 210 217 240 257 261 374 390
Epitopes
EIRFLRKIHEEEVRELQEQLAR
TQYEAMASSNMHEAEEWYRSKFAD
ENRITIPVQTFSNLQIRE
Clones
BD multi
3E10
5C10
BD multi
GA5
C
Human astrocyte trauma
Trauma
Cells
Fluid
kD
75
50
37
25
20
15
10
3E10
BD multi
5C10
GA5

Figure 3 (A)

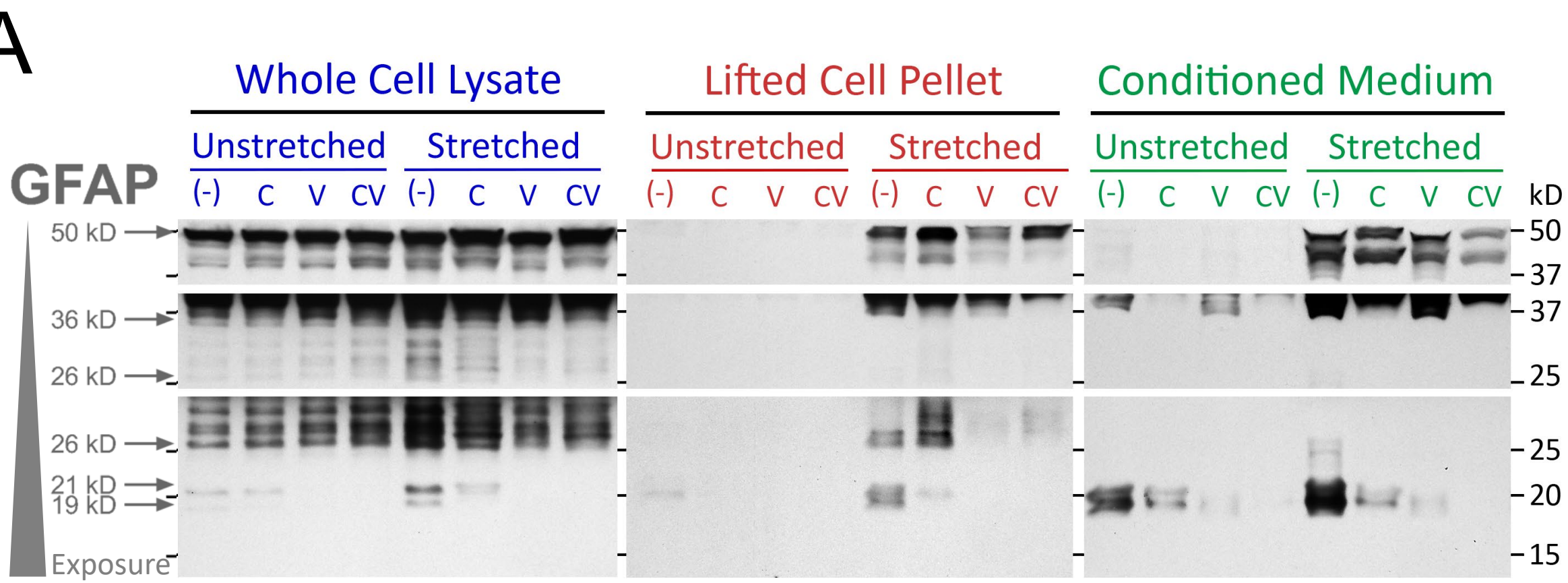
A
Whole Cell Lysate
Lifted Cell Pellet
Conditioned Medium
Unstretched
Stretched
Unstretched
Stretched
Unstretched
Stretched
GFAP
(-) c v cv (-) c v cv
(-) c v cv (-) c v cv
(-) c v cv (-) c v cv
kD
50 kD
36 kD
26 kD
26 kD
21 kD
19 kD
Exposure
50
37
37
25
25
20
15

Figure 3

B

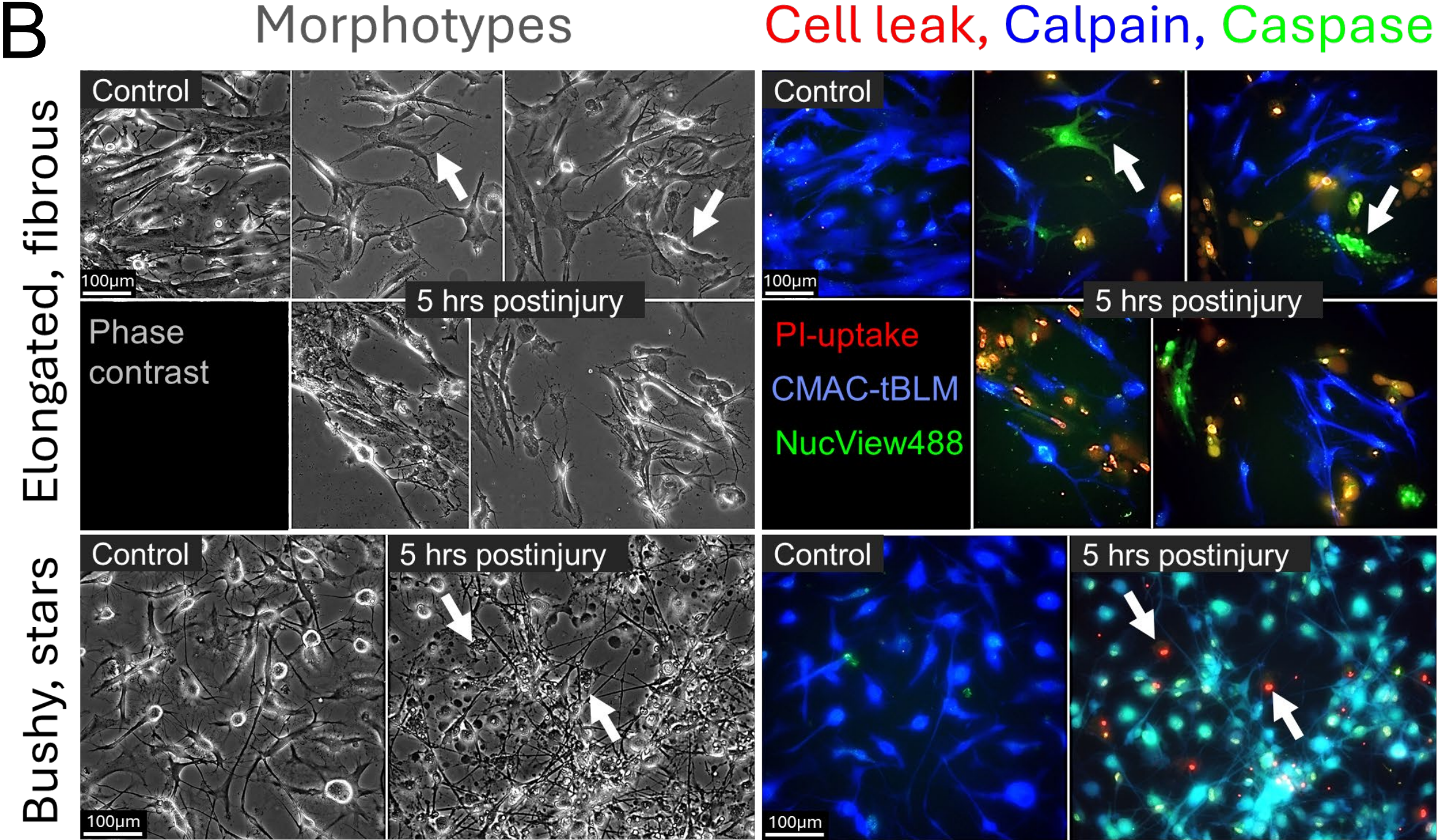
Morphotypes
Cell leak, Calpain, Caspase
Elongated, fibrous
Bushy, stars
Control
5 hrs postinjury
Phase contrast
100µm
PI-uptake
CMAC-tBLM
NucView488

Figure 3(C)

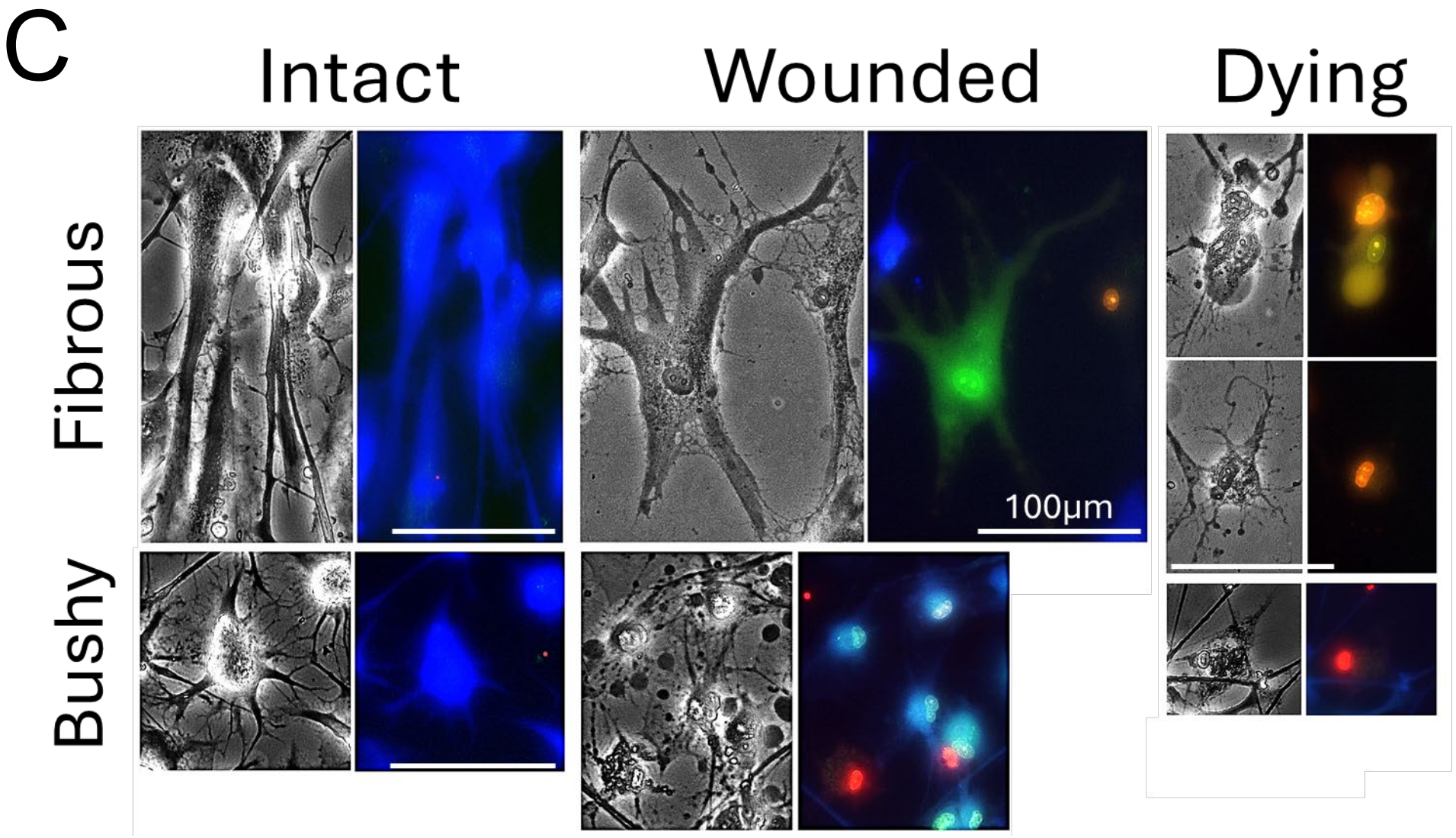

Figure 4

A

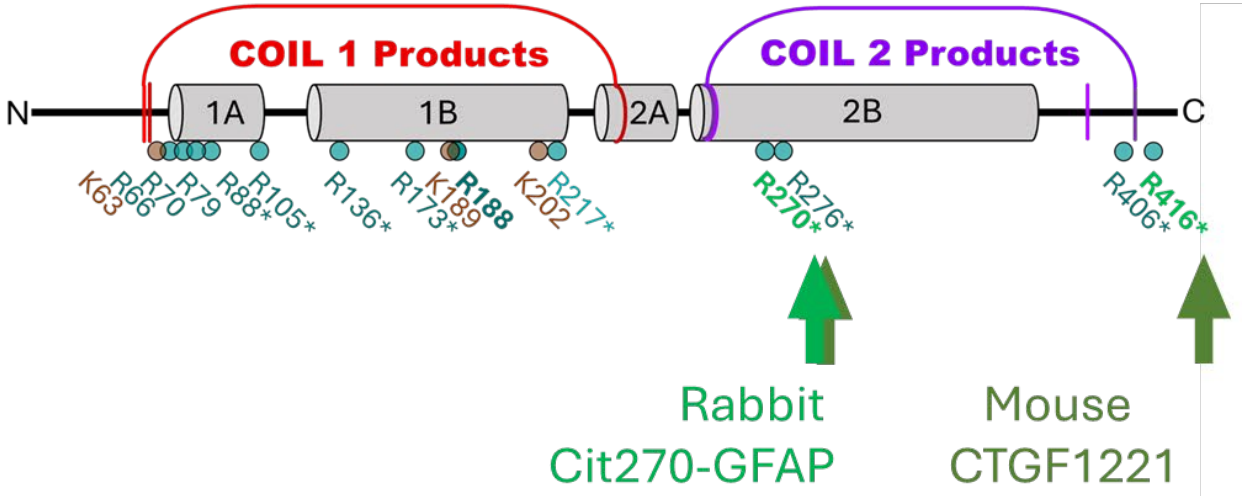

- 13 Citrullinated arginine residues
- 5 Acetylated lysine residues

B

Citrullinated GFAP Unmodified GFAP

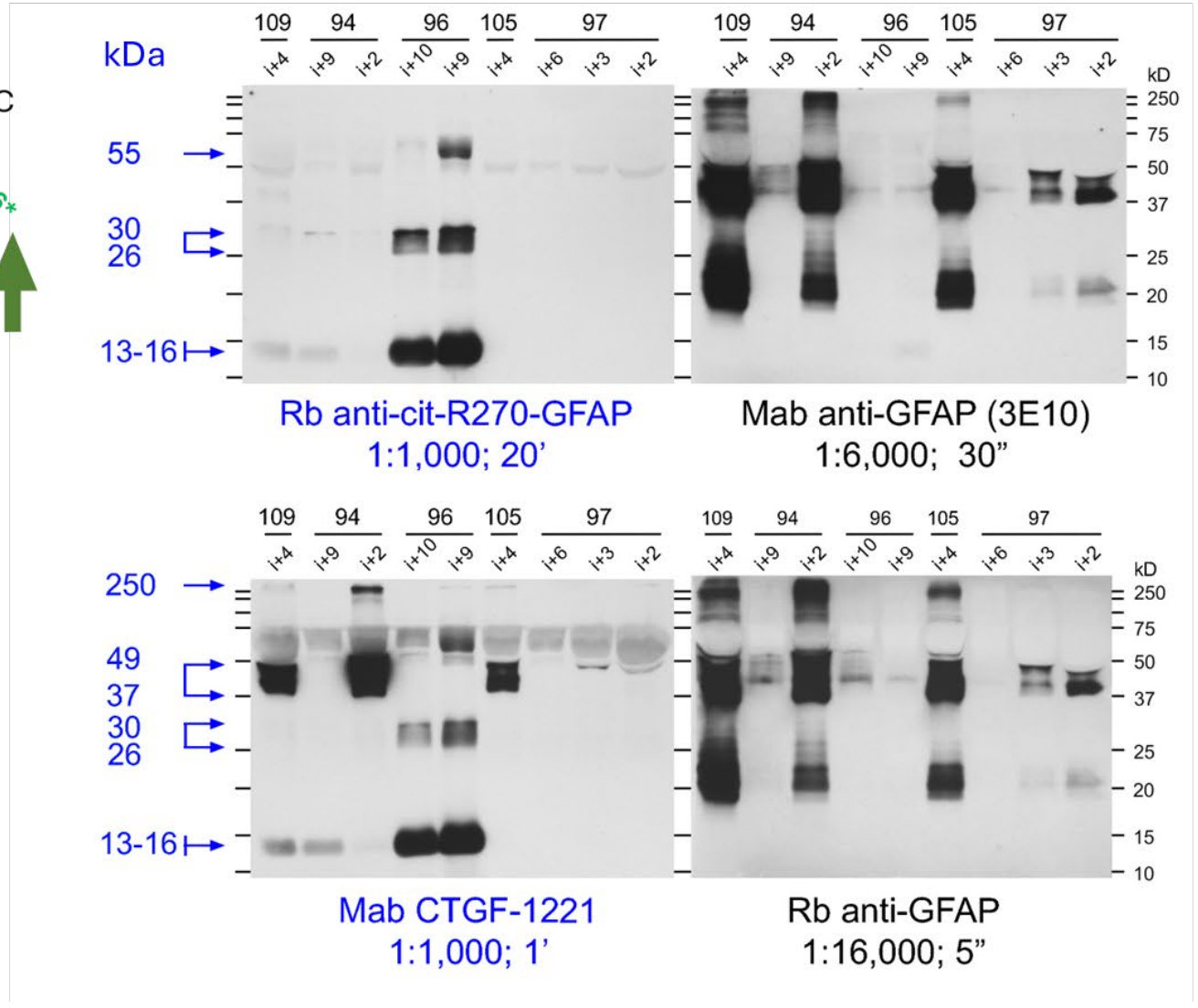

Figure 5

A

Control

Trauma

Unstretched

5 hrs post-stretch

24 hrs post-stretch

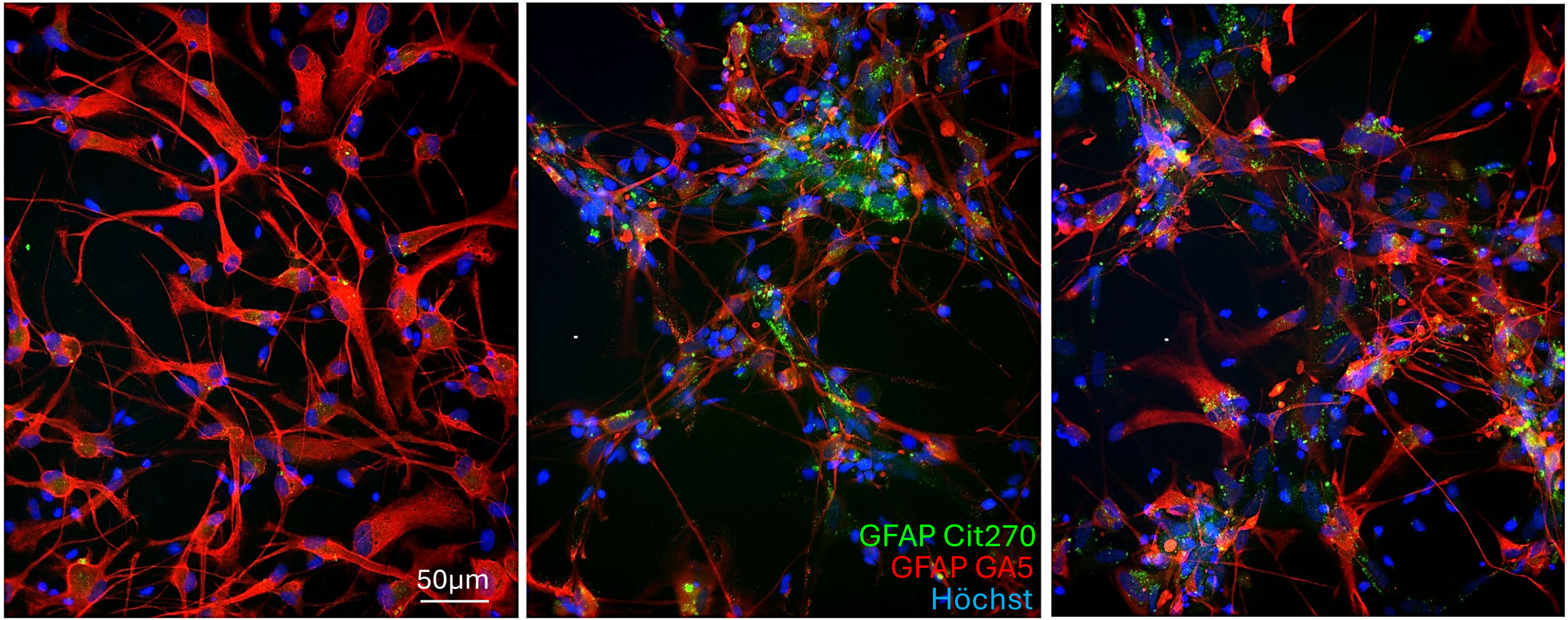

Figure 5 (B)

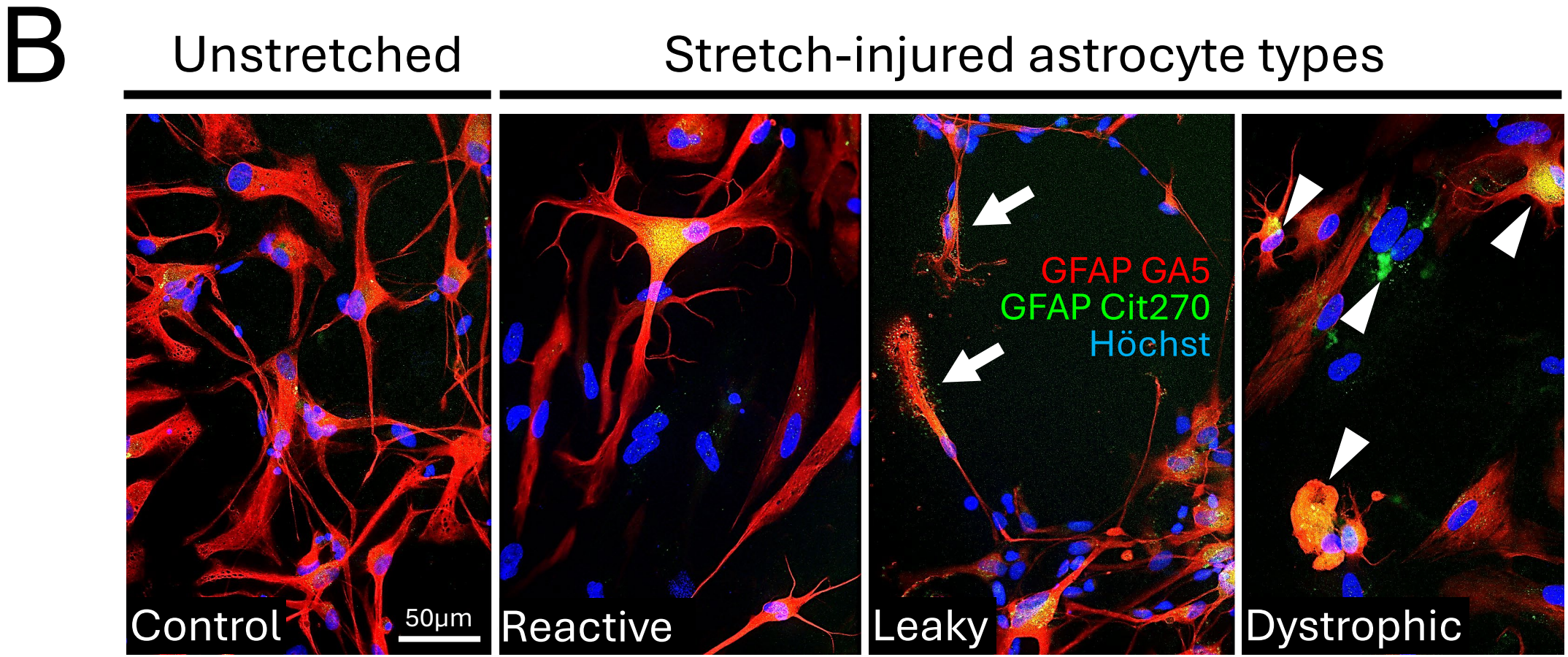
B
Unstretched
Stretch-injured astrocyte types
GFAP GA5
GFAP Cit270
Höchst
Control
50µm
Reactive
Leaky
Dystrophic

Figure 6

A

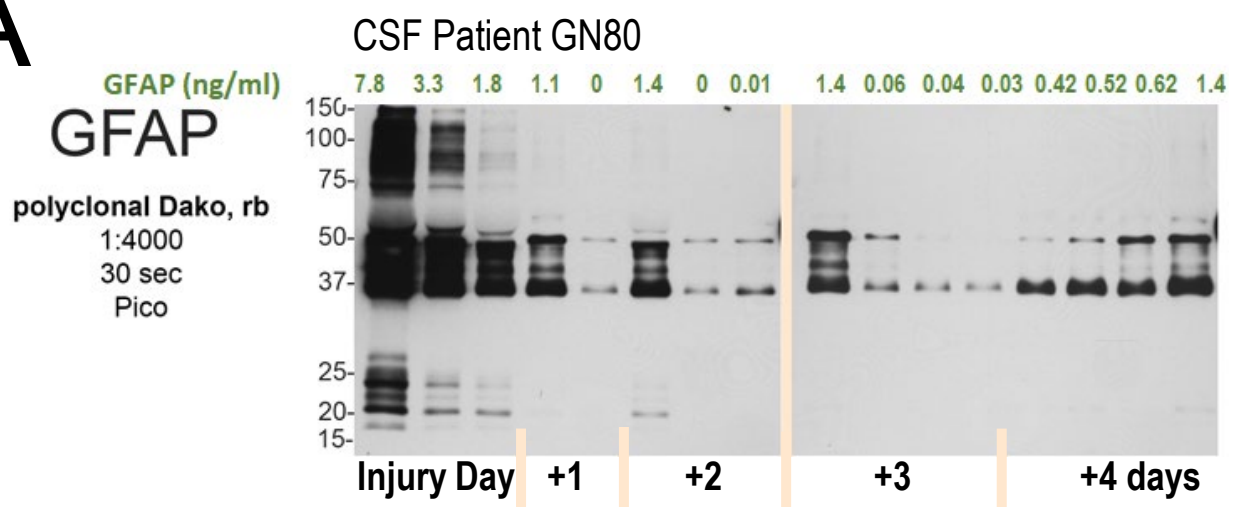
CSF Patient GN80
GFAP (ng/ml)
GFAP
polyclonal Dako, rb
1:4000
30 sec
Pico
7.8 3.3 1.8 1.1 0 1.4 0 0.01 1.4 0.06 0.04 0.03 0.42 0.52 0.62 1.4
150
100
75
50
37
25
20
15
Injury Day
+1
+2
+3
+4 days

B

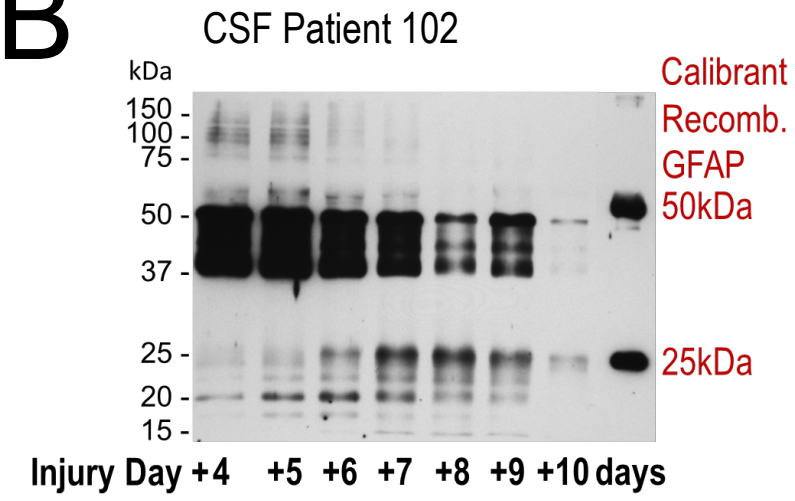
CSF Patient 102
kDa
150
100
75
50
37
25
20
15
Calibrant
Recomb.
GFAP
50kDa
25kDa
Injury Day +4
+5
+6
+7
+8
+9
+10 days

C

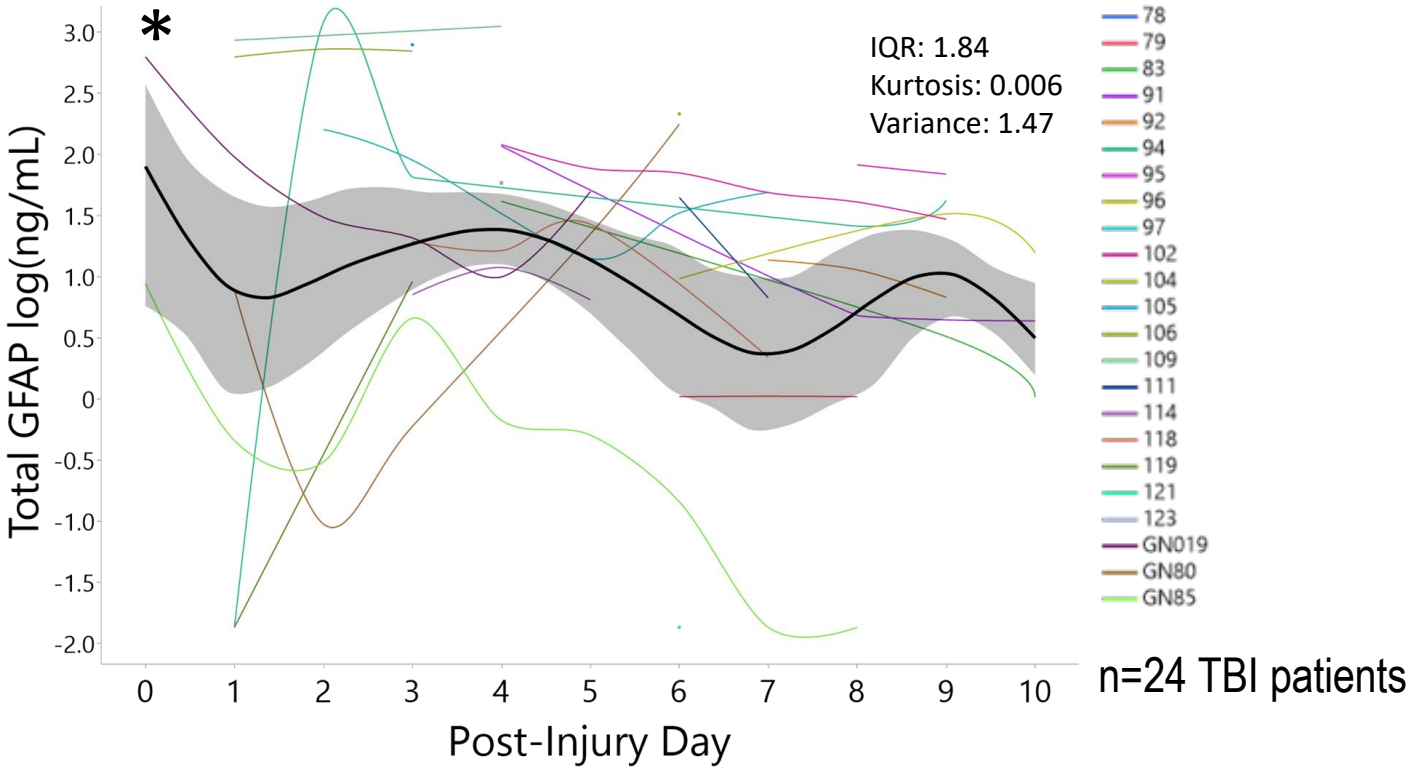
*
IQR: 1.84
Kurtosis: 0.006
Variance: 1.47
Total GFAP log(ng/mL)
3.0
2.5
2.0
1.5
1.0
0.5
0
-0.5
-1.0
-1.5
-2.0
0
1
2
3
4
5
6
7
8
9
10
Post-Injury Day
78
79
83
91
92
94
95
96
97
102
104
105
106
109
111
114
118
119
121
123
GN019
GN80
GN85
n=24 TBI patients

Figure 6 Continued

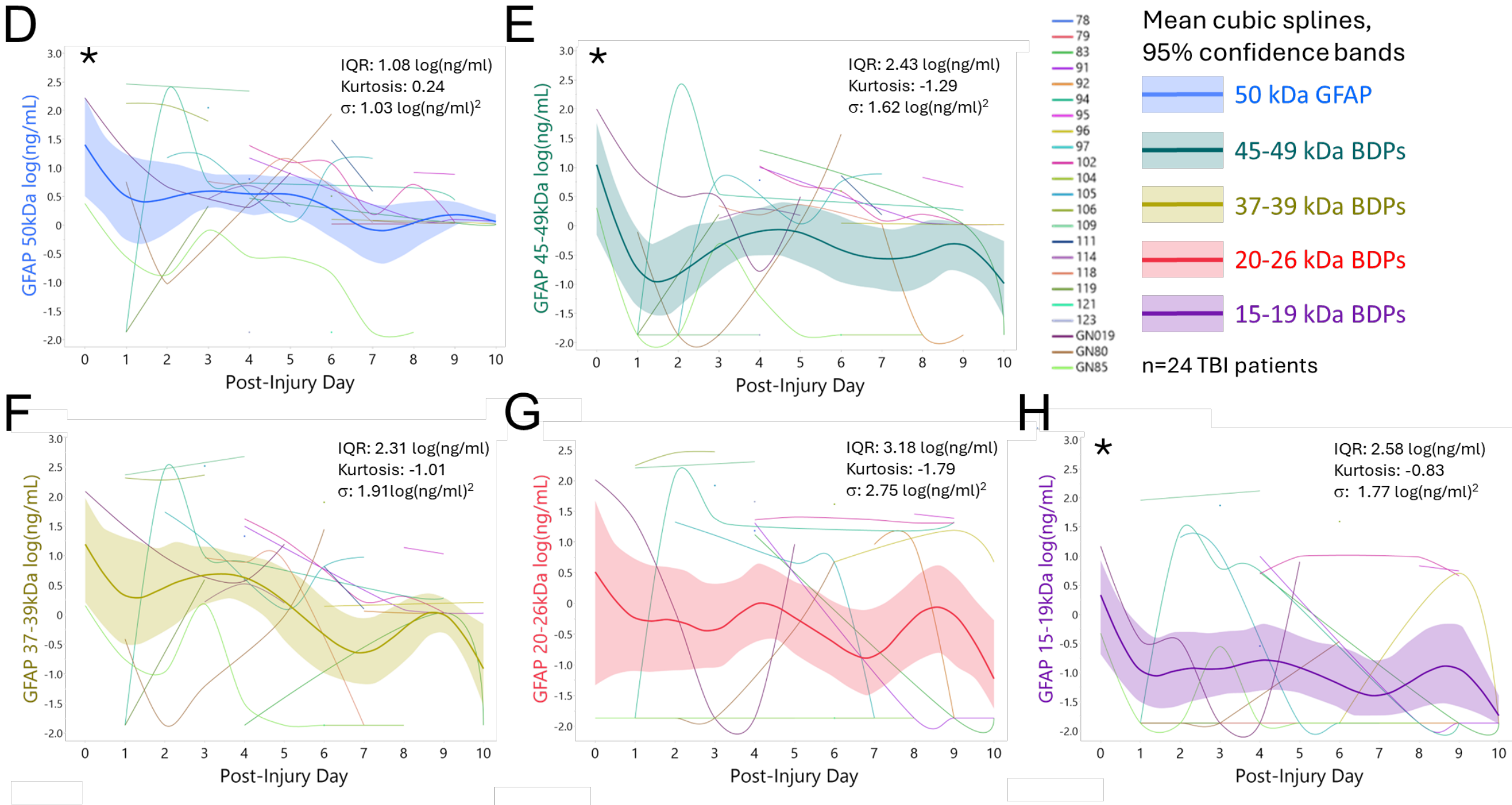

Figure 7

A

Pearsons correlation coefficients between GFAP proteoforms

	45-49kDa	40-42kDa	37-39kDa	20-26kDa	15-19kDa
50kDa	0.575	0.637	0.822	0.604	0.529
45-49kDa		0.596	0.589	0.413	0.422
40-42kDa			0.726	0.549	0.363
37-39kDa				0.714	0.567
20-26kDa					0.685
15-19kDa					

B

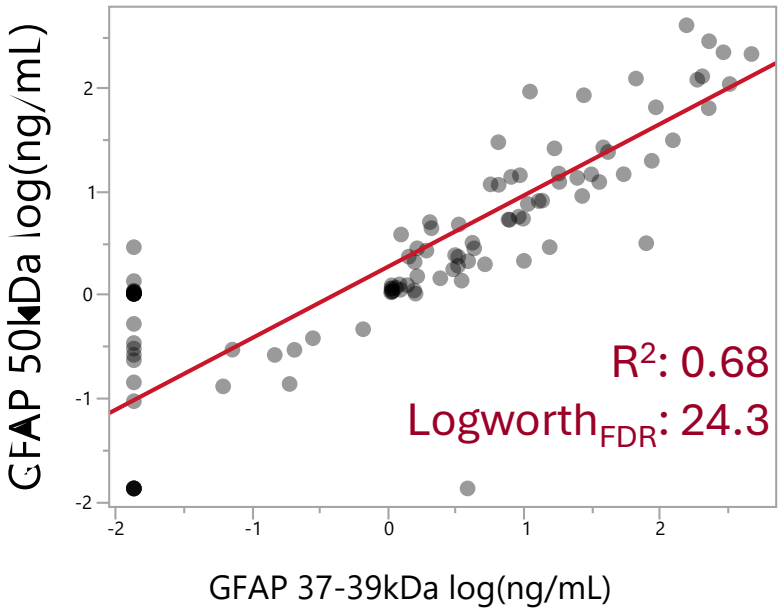

C

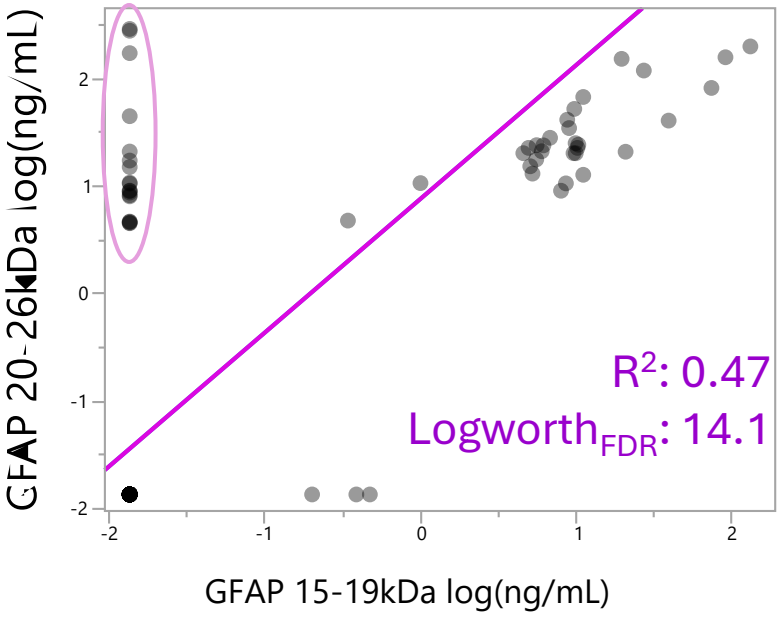

Figure 8

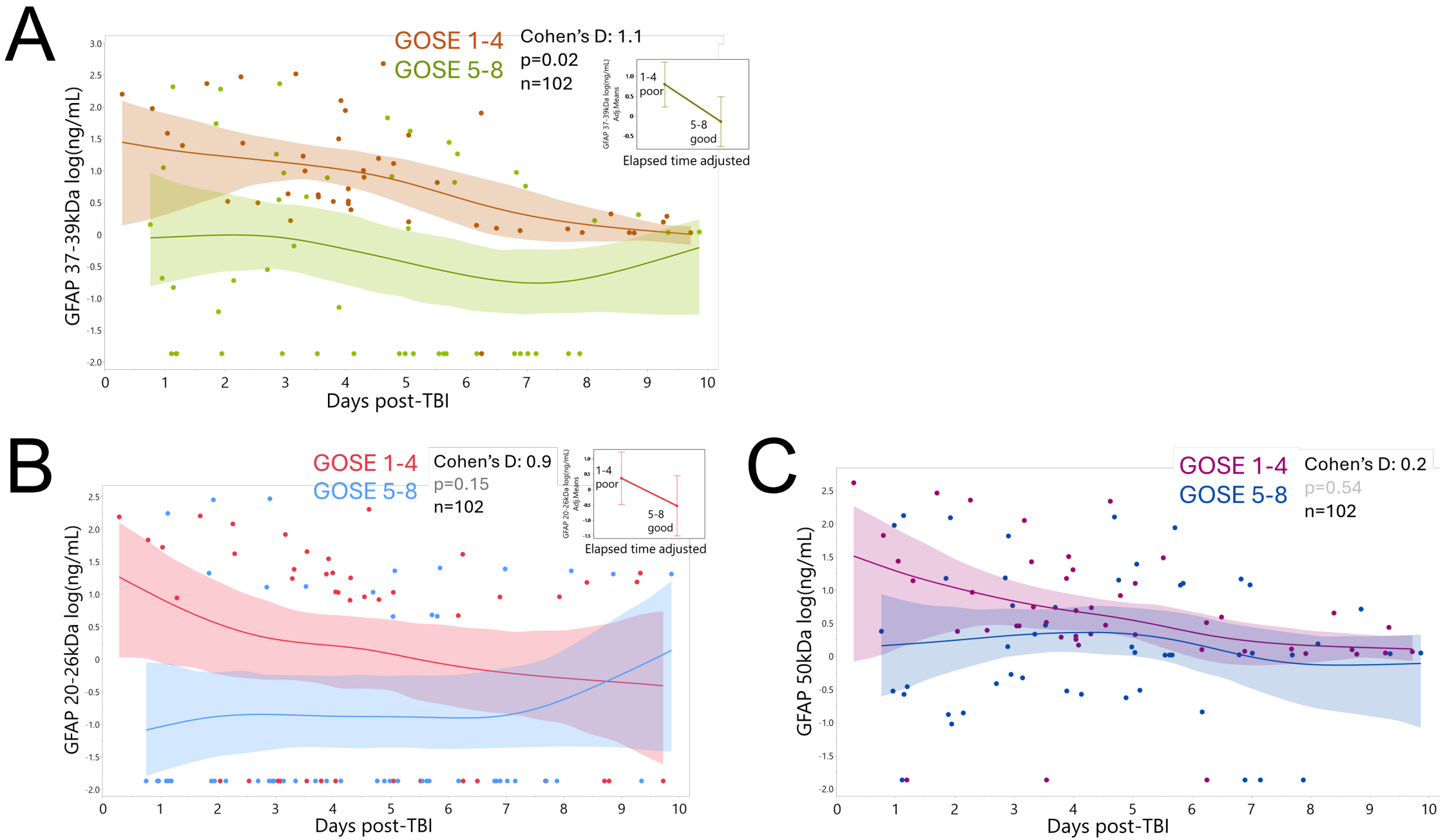
A
GOSE 1-4
GOSE 5-8
Cohen's D: 1.1
p=0.02
n=102
1-4
poor
5-8
good
Elapsed time adjusted
GFAP 37-39kDa log(ng/mL)
Days post-TBI
B
GOSE 1-4
GOSE 5-8
Cohen's D: 0.9
p=0.15
n=102
1-4
poor
5-8
good
Elapsed time adjusted
GFAP 20-26kDa log(ng/mL)
Days post-TBI
C
GOSE 1-4
GOSE 5-8
Cohen's D: 0.2
p=0.54
n=102
GFAP 50kDa log(ng/mL)
Days post-TBI